Summer 2012

# Comparison of experimental results of horizontal kaplan turbine with computational fluid dynamics

Vijaya Bijukchhe
*University of Iowa*

# COMPARISON OF EXPERIMENTAL RESULTS OF HORIZONTAL KAPLAN TURBINE WITH COMPUTATIONAL FLUID DYNAMICS

by

Vijaya Bijukchhe

A thesis submitted in partial fulfillment
of the requirements for the Master of
Science degree in Civil and Environmental Engineering
in the Graduate College of
The University of Iowa

July 2012

Thesis Supervisor: Professor Larry J Weber

Graduate College
The University of Iowa
Iowa City, Iowa

CERTIFICATE OF APPROVAL

_____

MASTER'S THESIS

_____

This is to certify that the Master's thesis of

Vijaya Bijukchhe

has been approved by the Examining Committee for the
thesis requirement for the Master of Science degree in
Civil and Environmental Engineering at the July 2012 graduation.

Thesis Committee: _____

Larry J Weber, Thesis Supervisor

_____

A. Jacob Odgaard

_____

Joseph Longo

To my loving parents

**ACKNOWLEGDEMENTS**

I would like to thank my Advisor Larry J Weber for giving me the opportunity to work in this project and his guidance and encouragement throughout the project. My sincere gratitude to Joseph Longo who helped me understand the experimental set up and whose constant motivation helped me work deeper in the research. I am thankful to Dr Edward Bennett for helping me with CFX. I would like thank Marcela Politano for helping me to learn Gridgen from scratch and being available whenever I faced problems with simulations.

I would like to express my gratitude to Professor Dr Pablo Carrica for guiding me with hydrodynamics of the flow.

I would like to thank my lab mates Antonio and Michael for giving me their precious time to help me with Gridgen.

I am grateful to all my friends in IIHR lab who created such a pleasant environment.

My sincere thanks to Liza D, who always gave me constructive feedbacks and motivated me till the end of this thesis.

I would like to acknowledge Sijal for his support. Also, to Ligaj, Srijana and Umesh who were always there for me.

## ABSTRACT

Hydropower has been the source of renewable energy for more than a century leading to reduction in burning of fossil fuels which has impact on the environment. More and more efficient hydro turbines have been developing for the power production with focus on the hydrodynamic behavior of the turbines. Emerging numerical codes specially designed to evaluate the efficiency of the turbine these days has made design of turbine a step ahead.

This project is contracted by AMJET Turbine System to evaluate the hydrodynamic, electrical and mechanical properties of a turbine prototype scaled to 1:7.828. The test stand was installed at the Hydraulic Model Annex#2 and the experimental fluid dynamics and data acquisition was performed by Joseph Longo, Research Engineer in IIHR - Hydroscience & Engineering.

The work on this thesis describes the numerical simulation of the prototype turbine at full load and partial load condition and comparison of the result with the experimental values for 30 feet of head at the runner outlet. Gridgen V15 and ANSYS Turbogrid has been used for high density mesh generation with total nodes of 1.3 million and ANSYS CFX 12.1 has been used to perform steady state analysis with backward Euler Scheme and Shear stress Transport as a turbulence model. Simulated results seemed to be best compared with experimental results for the optimum point and over predicted for the over load condition. Therefore, another set of simulations were run for cases where the turbine was making maximum power at heads from 20 ft to 50 ft. For

these values the output from the simulation follows the curve nature of the experiment. Total pressure on the mid span of the blade shows pressure below vapor pressure at the suction side of the blade at the leading edge which is due to the high flow velocity which creates low pressure at those regions.

## TABLE OF CONTENTS

## LIST OF TABLES

## LIST OF FIGURES

# CHAPTER 1 INTRODUCTION

Various sources of energy such as coal fossil fuels emit greenhouse gases which lead to global warming and depletion of the ozone layer. This has caused a negative impact on the environment with pollution due to burning of fossil fuels. Energy production through this means is still prevalent globally. But these sources are nonrenewable and will deplete at some point in the future (Kokubu et al., 2011). Hydropower has been the source of energy which is renewable and nonpolluting with the operational life of about 100 years. If we look into the global hydropower scenario, theoretical potential of worldwide hydropower is 2,800 GW, about four times greater than 723 GW that has been exploited now. Hydropower contributes about ten percent of energy production in the United States. A few decades ago hydropower contributed 40% of the electricity generated. Now the number has declined as other sources of energy, coal and nuclear have increased in large number. The energy production through the development of hydropower can be doubled to its existing production if the potential sites can be developed but due to social and environmental constraints these sites have not been considered for development.

There are thousands of dams in the US which are built for the purpose of flood mitigation and navigation. Only 3% of 80,000 dams in US have hydropower facilities (usbr.gov). Huge amounts of water stored in these dams have large untapped energy. Water falling through the spillway of these dams carries large amounts of kinetic energy which can be harnessed to produce renewable energy.

The principle of hydropower is extraction of potential energy from nature to convert it into mechanical energy and then to electrical energy by utilizing the head available and the discharge. Equation 1.1 shows the calculation of magnitude of the power developed.

$$P = n\rho gQH \ldots\ldots (1.1)$$

Here,

P = Power developed (watts)

n = Efficiency of the turbine

ρ= density of the water ($kg/m^3$)

g = Acceleration due to gravity ($m/s^2$)

Q = discharge ($m^3/s$)

H = available head (m)

Development of the turbine began in the 18th century when the steam turbine was developed as first reaction turbine. Various types of turbine have been developed since then which operates for high, medium and low head applications. Figure 1.1 shows different types of turbine and their application.

Figure 7.6 shows the slice of the passage of the runner at the mid span in a 3D view. This 3D plane is unwrapped into a 2D plane to view the pressure contours and velocity streamlines more clearly. Figure 7.6 is shown in cartesian coordinates. Pressure contours and velocity streamlines at the mid span of the runner blade is shown in Figure 7.8 and 7.9. Only one runner blade is shown in the diagram as similar flow exists in all

the passages due to periodicity.Figure 7.7 shows the sliced surface of the blade in a 2D plane showing leading and trailing edge and pressure and suction side.

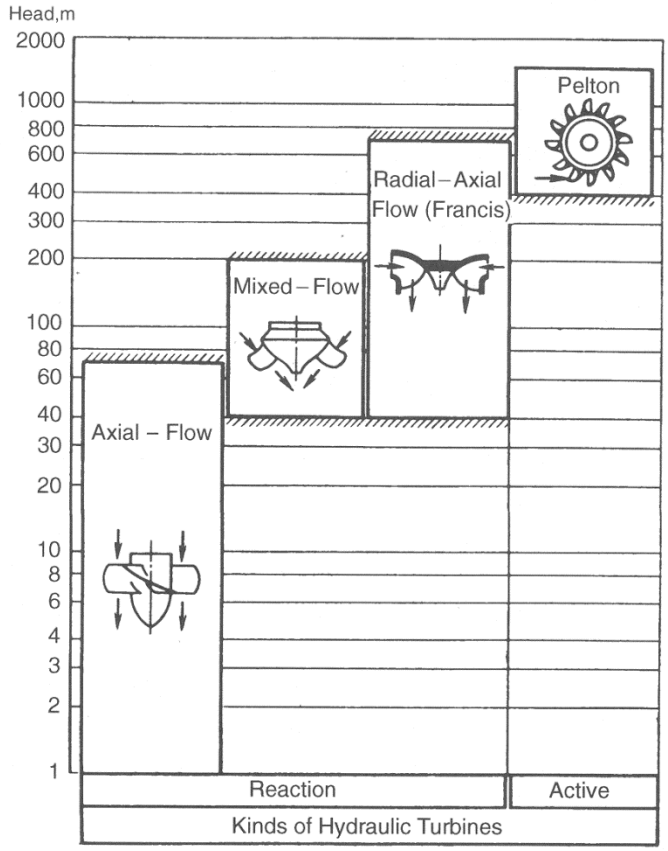


**Figure 1.1 Application of turbines of different kind**

The difference between Kaplan turbine and Pelton turbine is that Kaplan turbines utilizes pressure energy and kinetic energy of water whereas Pelton turbine utilizes only the kinetic energy of the water so it requires high head for the power generation (Grigori Krivchenko, 1994).

The turbine's hydraulic capacity is determined by the specific speed of the turbine which is given by equation 1.2. It is the speed of a turbine of specific size which generates a power of 1 hp at 1 m of head.

$$N_s = \frac{N \times \sqrt{Q}}{(g \times H)^{0.75}} \dots\dots (1.2)$$

An axial turbine being low head and high discharge turbine will have high specific speed. High specific speed of a turbine can be subjected to cavitation as well. The cavitation coefficient depends upon the value of specific speed. It can be calculated from the equation 1.3.

$$\sigma = \frac{(N_s + 30)^{1.8}}{200{,}000} \dots\dots (1.3)$$

Where,

σ is cavitation index and Ns is specific speed of a turbine.This equation clearly explains that cavitation is directly proportional to the specific speed. Therefore high head plant demands low specific speed turbine to make it free from cavitation (Grigori Krivchenko, 1994).

Amjet Turbine System developed the idea of producing a horizontal Kaplan turbine which can be installed in the dams and sites where low head and high discharge is available. The runner blades are attached with the shroud of the turbine which makes the generator and turbine as an integral part. As the size of the turbine is relatively smaller than other types of turbine, such a turbine will have low production and installation cost which ultimately reduces the size of the powerhouse as well. The

design of this turbine was to achieve 300Kw of power at 10 feet net head and 450 cubic feet of volume flow.

Model testing of the turbine is a conventional approach to find its performance. Any change in the model with fabrication and testing can result in huge cost. Also, it lacks to find out several factors like recirculation, vortex shedding and cavitation that govern the performance of the turbine (Prasad Vishnu et al., 2009). With the development of numerical simulation, not only the flow prediction in a turbine has become easier, but it has also become possible to validate the experimental data. With the recent advancement of numerical modeling in the field of turbomachine, it is now possible to account for complex flow phenomena. Though experimental verification of the performance of hydro turbines via numerical simulation is not new, such research is being done for the first time in the IIHR lab. Hence, in this study we have conducted a numerical simulation for the verification of the performance of the AMJET turbine with respect to experimental study of the prototype that was simultaneously carried out.

### 1.1 Objectives

The objective of this project is to perform the CFD simulation of the 8-inch model axial turbine using simulation software ANSYS CFX to develop the performance curve and determine the turbine efficiency at working load condition. Following are the specific objectives of this project:

1) To use experimental data and develop characteristic curves of the turbine working on 30ft of net head.

2) To plot the performance curve to compare the overall power, torque and discharge of a turbine from numerical simulation with the experimental data available from the physical test of the prototype turbine.

## 1.2 Methodology

The study of the hydrodynamics of the turbine is conducted by using ANSYS CFX using Shear stress transport Model. This model has widespread use for design, optimization and validation with the experimental data of the hydro turbine. (Prasad Vishnu et al., 2009). Following are the activities that have been conducted for the fulfillment of this study.

1) Literature review of CFD simulation of the hydro turbine and study of different models used for the simulation.
2) Mesh generation of the 1:7.828 reduced scale horizontal Kaplan turbine geometry developed by Mechanical Solution Inc. as contracted by Amjet Turbine System LLC. The meshing software used was Pointwise Gridgen V15 and ANSYS Turbogrid 12.1 to generate high quality meshes.
3) Mesh independency study is carried out to check the sensitivity of the mesh generated to get the required results.
4) Collect and analyze the data of the experiment of the model conducted at IIHR-Hydraulic Annex # 2.
5) Flow analysis is carried out at steady state using stage interface which requires only one rotor and one stator blade to model. Using periodicity in a single

passage, it minimizes total size of the mesh which ultimately reduces computational time and memory storage required.

6) Perform numerical analysis using interpolated experimental data. The data used are from the curve developed for 30 feet of head across the rotor and the peak power production at different head of the turbine.

7) Post processing of result in CFX post and Tecplot to analyze the result and validate with the experimental data.

8) Discuss findings of the study and relate with the literature available in context of hydraulic simulation of turbine.

Much research has been carried out in the field of turbo machine to evaluate their performance and efficiency based on the physical processes occurring inside the machine. State of the art is reviewed to assess the models and assumptions used so far in the field of CFD. The following chapter deals with the literature review of papers related to the objectives that have been set by this thesis.

# CHAPTER 2 LITERATURE REVIEW

Turbines are regarded as the most significant component of any hydro power plant. They cover about 15 – 35 percent of the total project cost. Feasibility of the project depends on the cost of its components. Many laboratory experiments were carried using physical model to know the hydrodynamic behavior of the machine. Physical modeling has been one of the methods in knowing the behavior of the turbine but has been a costly and time consuming technique. It is very important to understand about how energy is transferred and rotor stator interaction takes place in a turbine beforehand to predict the behavior of the turbine so as to make cost effective design (Motycak et al., 2010). Since past two decades computational fluid dynamics has become a powerful tool in analyzing the flow field of complex turbo machines and has been used extensively during the study for design of the turbine in order to optimize the design as well as to save time.

Various information regarding the real flow field can be gathered by numerical analysis and also accuracy of the experimental measurement can be checked through this analysis. Lukas Motycak et al (2010) conducted a model test as well as CFD analysis of the runner draft tube interaction in Blasko engineering focusing on the detailed measurement of the velocity at the downstream of the runner by differential probe measurement and the velocity measurement downstream of the draft tube by Particle Image Velocimetry (PIV) and good agreement was achieved between experimental and CFD results. Numerical analysis of the flow helped to alter the design of a draft tube for better performance (Motycak et al., 2010).

Two types of methodology are generally used for the simulation of the turbine depending upon the required objectives. Steady state simulation has been used to determine the efficiency of the turbine (Jain et al., 2010). The nature of flow in turbine is unsteady in nature due to rotating of the runner. Therefore unsteady state simulations are conducted to know the transient behavior of the flow and for the investigation of the pressure fluctuation in different component of the turbine and also the interaction between rotor and stator. Santiago et al employed steady and unsteady simulation for the numerical analysis of the Francis turbine. Boundary conditions were mass flow inlet and opening with pressure outlet with solid surfaces as walls for both types of simulation. He stated that this type of boundary condition represents real flow in the turbine. He developed the hill chart of the Francis turbine to determine its efficiency by 25 simulations with five different openings of guide vanes. Experimental measurements were carried out by placing dynamic pressure sensors in guide vanes runner blades and draft tube. The results from the experiments were matched with the numerical values and they were found to be satisfactory for optimum loading conditions and off load condition (Laín et al., 2012).

Gagnon et al presented unsteady interaction of a rotor and a stator in a propeller turbine. His works mainly focused on the interaction of rotor and stator and find the relation of runner blade torque, guide vanes forces and fluctuating pressure as a function of operating conditions. He stated that a numerical simulation provides nonphysical results for the cases that are situated much off from the peak point. Accordingly, in his study he considered three cases with peak and two off peak conditions very close to peak point. The transient simulations indicated forces fluctuations at partial load and overload conditions. He further explained that these fluctuations might be caused by the

gap between rotor and stator interface which allows space for damping and by low operating head of the machine. He concluded that for the flow to be perfect, mesh should be geometrically similar at the interface between rotor and stator so that the flow information if transmitted from stator to rotor without interpolation (Gagnon and Deschênes 2007).

In literature different turbulent modeling were found being used in simulating flow in hydro turbine. Most of the work done has used wall function approach which does not resolve boundary layer. Though these approaches seem to save computational time as mesh need not be refined at the boundary layers, they are often not validated with the detailed measurements of velocity and pressure. Thus, low Reynolds's number turbulent model are being used to resolve the viscous sub layer and transition phenomena occurring in the turbine which is very important if there is hub and tip clearance in the turbine (Nilsson and Davidson 2003). Among the turbulence model, k-w shear stress transport model has been found to give better convergence and turbine performance compared with standard k-e, Renormalization group (RNG) k-e (Jain et al., 2010;Kokubu et al. 2011). SST model has been successful in giving accurate results for cases where there are adverse pressure gradient flows and where separation of flow occurs.

Boundary condition represents the known computational values within the ends of the spatial domain for any temporal variations. In most of the literature, mass flow inlet, static pressure outlet and total pressure inlet and mass flow outlet boundary conditions has been used for turbine simulation. Mass flow inlet and static pressure outlet is considered as most robust BC (Advice on flow modeling on CFX-5). Zoran Carija et al (2008) used total pressure inlet and static pressure outlet as their boundary

condition for validating Francis turbine with the CFD simulation. The total pressure inlet is defined as the sum of static and dynamic component.

$$P_{total} = P_{st} + \frac{1}{2}\rho v^2 \ldots\ldots (2.1)$$

As volumetric flow rate is not known, total pressure at the inlet was calculated by following equation

$$p_{total,in} = \rho g \left((Z_{hw} - Z_1) - H_{loss(HW-in)}\right) \ldots\ldots (2.2)$$

$H_{loss(HW-in)}$ is head loss between head water level and turbine inlet section. The volumetric flow after every 10 iteration was used in above equation to get new total pressure and solver was run till solution converged. The static outlet BC was taken at tail water level. They performed unsteady state Naviar Stokes simulation and validated the result with the experimental data (Čarija, Mrša, and Fućak 2008).

Steady state analysis done in turbine research has given fairly accurate results that satisfy the research objectives. All the transient effects are removed in this analysis as the fluxes are circumferentially averaged when moving from rotor blade passage to the stationary passage. Unsteady analysis or transient analysis is performed when fluctuations of different variables are required for the analysis (Best practice Guidelines for Turbomachinery, 2011). Non uniformities in the flow are observed in draft tube and spiral casing due to the formation of vortex rope. These cases if solved with steady analysis will fail to provide true phenomena occurring in the system (Gagnon et al., 2008). Feasibility of hydropower plant is greatly dependent on the transient behavior of the turbine. During load rejection, unsteady behavior is highly observed in the turbine as well as in penstock and surge tanks (Liu et al., 2008). S Lui conducted transient

simulation at rated operating condition of the model Kaplan turbine and found pressure fluctuation in a draft tube inlet and predicted strong swirling flow in the draft tube. While in runaway transient analysis, back flow was observed in the draft tube in which vortex rope was likely to be observed which creates pressure fluctuations (Liu et al., 2008).

Variation in the experimental and simulated data is caused by various factors. Vishnu et al stated that the variation may be caused by losses that are not fully accounted, errors in discretization of the governing equations and flow domains and considering only a part of the geometry (Prasad Vishnu et al., 2009).

The efficiency of the hydro turbine is determined by the loss coefficients. There are mainly two types of losses: mechanical loss which is due to the friction imposed by the rotation of the turbine and impact loss.

Cavitation is considered as one of the harmful effect in the turbine which decreases its performance with corrosion of its material. The cause of cavitation is due to decrease of local static pressure below the vapor pressure which occurs when high turbulent flow passes through the turbine runner (Drtina and Sallaberger, 1999). Water bubbles are created which with the high velocity explodes creating shock waves which can yield the strength of the material. These frequently occurring shock waves causes the material to  elastic and plastic deformation ultimately causing the formation of cracks on the turbine blades (Hart et al., 2007).

Cavitation mostly occurs at low pressure location which is in most of the cases in the suction part of the turbine and at off design condition it has been observed on the leading edge of the turbine. Hence, high relative velocities are avoided so that cavitation can be avoided while designing for efficient turbines (Drtina and Sallaberger, 1999).

The literature review provided a thorough understanding of overall numerical simulation of turbine. Besides, it made familiar with different turbulent models that can be used depending upon required objective. Chapter 3 deals with CFD model development of the Amjet Turbine with the understanding of the state of an art for simulation of hydro turbine.

# CHAPTER 3 CFD MODEL

## 3.1 Introduction

Computational fluid dynamics is widely being used to analyze the flow field since last 20 years. It's capability to solve complex flow phenomena with enhanced software have made it popular in several fields. X-Y-Z momentum of Navier Stokes equation and continuity equation is solved numerically. These are differential equations of complex fluid dynamics which requires discretization of the flow in order to solve them. There are several methods of discretization that have been used. Finite volume, finite element and finite difference are the three methods that are currently being used as discretization method for CFD analysis. Among these, finite volume method is used in CFX in which volume is developed by generating mesh to solve the partial differential equations of mass, momentum and energy (John D Anderson, 1995).

## 3.2 Hydrodynamics

The fundamental conservation laws governing the fluid flow in the turbine are:

Conservation of mass: For any period of time mass of a system will remain conserved. The net mass flow out of the system must be equal to rate of decrease of mass inside the system. Following equation is the partial differential equation form of the continuity equation.

$$\frac{\partial \rho}{\partial t} + \nabla.(\rho V) = 0 \ldots\ldots \quad (3.1)$$

Conservation of momentum: Net force applied on the moving fluid is equal to the mass of an element times its acceleration. Forces acting on the fluid element are body forces which includes gravitational, electric and magnetic forces and surface forces which are due to the pressure distribution acting on the surface and the shear stress and normal stress distribution due to outside fluid. Following is the equation for the conservation of momentum.

$$\rho\left[\frac{\partial V}{\partial t} + V.\nabla V\right] = F_b - \nabla_p + \mu\nabla^2 V + \frac{\mu}{3}\nabla(\nabla.V) \ldots\ldots \quad (3.2)$$

These equations are solved for the finite volume element as developed with the meshing tool and analytical solutions are obtained as required for the study.

With proper boundary condition and quality mesh, CFD is able to solve both laminar and turbulent flows. Laminar flows are easier to solve compared with the turbulent flows as turbulent flows are unsteady in nature which are developed at high Reynolds's number. Small scale and large scale eddies are developed which are three dimensional and random in space and time. There are flow models developed to solve turbulent flows. Depending upon the requirement of the results, flow models are selected and computational power required for the simulations depends on these selected models.

Turbulence modeling is solved by Reynolds's Averaged Navier Stokes (RANS) equation, large eddy simulation (LES) model and direct numerical modeling (DNS). Direct numerical simulation gives very accurate result by solving all time and space scales. However, the grids needs to be very small to resolve spatial and temporal scales and consumes large computational time. Reynolds's Averaged Navier Stokes model solves by time and space averaging. This model provides pretty good result but fails to give accurate results for transient simulation where variables vary with time.

### 3.3 Turbulence modeling

Large scale and small scale eddies are generated due to turbulence in the flow. Various turbulence models have been developed to capture the effect of these unsteady turbulent eddies. These models are based on Reynolds's Averaged Navier Stokes equation which is the sum of statistically averaged component and fluctuation component. Reynolds's Averaged Navier Stokes equation can be written as

$$U_i = \bar{U}_i + U'_i \ldots\ldots (3.3)$$

Here, $\bar{U}_i = meanvelocity$, $U'_i = fluctuationcomponent$

$$\frac{\partial U_i}{\partial x_i} = 0$$

$$\frac{\partial(\rho U_i)}{\partial t} + \frac{\partial(\rho U_i U_j + \rho\overline{U_i U_j})}{\partial x} = -\frac{\partial \bar{p}}{\partial x_i} + \frac{\partial \overline{\tau_{ij}}}{\partial x_j}$$

Here,$\bar{\tau}_{ij}$ are the mean viscous stress tensor components

$$\bar{\tau}_{ij} = \mu\left(\frac{\partial u_i}{\partial x_j} + \frac{\partial u_j}{\partial x_i}\right) \ldots\ldots (3.4)$$

### 3.4 Shear Stress Transport Model

Shear stress transport model is the combination of k-e and k- ω model. These two models are two equation turbulence models whose transport equations are solved along with mass and momentum equations. The k denotes turbulent kinetic energy, e denotes rate of turbulent dissipation and ω denotes specific dissipation. The limitations of these two models are incorporated in SST model. k-e model over predicts the shear stress in

adverse pressure gradient flows and it requires near wall modification as well but still it cannot capture proper flow separation in the turbulent flow. For proper flow prediction in the near wall layers k- ω model provides better accuracy then k-e model. However it also fails to predict for separation induced by high pressure. Shear stress transport model was developed to overcome the limitations of these two models. With the introduction of blending factors, k- ω and k-e zones are selected automatically without user interaction at near wall region and away from the surface respectively. This model gives accurate results for the flows with adverse pressure gradient like in airfoils and flows with separation. Hence, Shear stress transport model is reliable to be used for turbines (Menter, 1994).

### 3.5 Wall Function

Three sub layers exist at the near wall region of the fluid flow. Viscous sub layer which is the innermost layer is almost laminar in nature as viscosity is more dominant. Then there is logarithmic layer where there is a mixing effect due to turbulence. In between these two layers there is another layer which is thin called buffer layer where both viscosity and turbulence have their effect.

Within these layers flow variables are changing rapidly. In order to account for the viscous effect and these rapid variations in the flow many models are developed which considers flow details in near wall regions. There are basically two methods to model the flow near the wall region. Wall function method is used when boundary layer is not resolved so the mesh need not be refined for this method which saves the computational time. Coarse mesh can used to model shear layers near the wall but this

approach neglects any effect due to viscosity in the viscous sub layer. Another approach is Low Reynolds's number method which uses very refined mesh near the wall and accounts for the viscous effect in the sub layer. Low Reynolds's number refers to the Reynolds's number of the viscous layer which is low and not of the system as a whole. In SST model automatic wall treatment method has been developed by CFX. When $Y^+$ is less than 6 it integrates to the wall and when y plus is equal to or greater than 30 it switches to standard wall function. In between $Y^+$ 6 and 30 it uses the blending function. The logarithmic relation for the near wall velocity is

$$u^+ = \frac{U_t}{u_\tau} = \frac{1}{k}\ln(Y^+) + C \ldots\ldots (3.5)$$

Here,

$$Y^+ = \frac{\rho \Delta y u_\tau}{\mu} \ldots\ldots (3.6)$$

$$U_t = \left(\frac{\tau_\omega}{\rho}\right)^{1/2} \ldots\ldots (3.7)$$

Where, u+ is the near wall velocity,

uτ is the friction velocity,

Ut is the known velocity tangent to the wall at a distance of $\Delta y$ from the wall, $Y^+$ is the dimensionless distance from the wall, τω is the wall shear stress, k is the Von Karman constant and C is a log-layer constant depending on wall roughness.

### 3.6 $Y^+$ Calculation

$Y^+$ value is an important parameter to properly address different turbulent phenomena of the flow. The value of y plus can be estimated to find out the wall distance which makes it easier to mesh the domain.

$$\mathrm{Re} = \frac{\rho U_{\mathrm{freestream}} \times L_{boundarylayer}}{\mu} \ldots\ldots (3.8)$$

Here,

ρ= density of the fluid

$U_{freestream}$ = velocity of free stream

$L_{boundary\ layer}$ = length of the boundary layer

We calculate the Reynold's number to estimate the skin friction from the following equation

$$C_f = [2\log_{10}(\mathrm{Re}_x) - 0.65]^{-2.3} \ldots\ldots (3.9) \text{ For Rex < 109}$$

This is Schlichting skin-friction correlation

Then wall shear stress is calculated using the following equation

$$\tau_\omega = C_f \frac{1}{2} \rho U^2_{\mathrm{freestream}} \ldots\ldots (3.10)$$

Frictional velocity is calculated by the following equation

$$U_* = \sqrt{\frac{\tau_\omega}{\rho}} \ldots\ldots (3.11)$$

Finally the wall distance is calculated with following equation

$$y = \frac{Y^+ \mu}{\rho U_*} \ldots\ldots (3.12)$$

The wall distance from the above formula is used to estimate tentative $Y^+$ value for the mesh generation ($Y^+$ Calculator).

### 3.7 Frame change

Interfaces between rotating and non-rotating component of the machine are specified based on multiple frame reference concept. Frame change available in CFX is frozen rotor, stage interface and transient rotor stator. Among these, stage interface is one of the simplest methods. This is the method of circumferential averaging where flow variables at the interface are averaged in a circumferential direction. Only one rotor blade needs to be modeled for this type of setting which saves huge computational time and memory but it neglects all the transient effects (Brost et al, 2003). Stage interface provides steady state solution. For unsteady rotor stator interaction, transient solution needs to be obtained. Transient analysis is carried out to know about flow variables at different time. Steady state solution ignores all higher terms that are time dependent while getting convergence.

### 3.8 Boundary Conditions

Boundary condition represents the known computational values within the ends of the spatial domain for any temporal variations. The inlet and outlet boundary conditions can be discussed as follows:

### 3.8.1 Inlet boundary condition

The inlet boundary conditions used in this simulation is total pressure which is the sum of static pressure which basically is the hydrostatic head at the inlet and dynamic pressure which is developed by velocity of the fluid at the inlet.

Total pressure = Static pressure + Dynamic Pressure

$$P_T = \rho g h + \frac{1}{2}\rho v^2 \ldots\ldots (3.13)$$

### 3.8.2 Outlet boundary condition

Static pressure is imposed at the outlet of the domain which is averaged over the area. While imposing outlet boundary condition, due to recirculation in the draft tube the fluid flows inside the domain. In order to prevent this, the solver creates a wall at the outlet. In most of the cases more than 20% of the area is created as wall. Therefore, the boundary condition is changed to opening type.

The shroud of the rotor also rotates with same speed as the blade so the whole domain is set to rotating boundary condition and other two domains as stationary boundary condition. All boundary walls are assumed to be smooth wall with no slip. As the geometry of the turbine possessed symmetry and similar flow conditions will be developed in other passages as well, periodic boundary condition was employed.

General grid interface (GGI) is used to connect the domain with different type of mesh and number of nodes. GGI connection has also been used to connect the domain with stationary frame and rotating frame with different mesh density and type.

### 3.9 Model setup

The objective of this thesis is to compare the power and efficiency developed by this axial turbine in laboratory with the computational method using CFX. Input data for the CFD were extracted from the experiment. From the contour plot of RPM vs. electrical power for different head, data were extracted for 30 feet of head. These data include pressure at four taps, mass flow rate, rotational speed, electrical power which will be input conditions on CFX.

The incompressible steady turbulent flow is considered for the passage of the modeled scale turbine. The continuity equations and Reynold's Averaged Naviar stokes equation is used along with SST model with automatic wall function. Advection scheme was set to high resolution with second order backward Euler for discretization. The flow is considered incompressible. The solver used was ANSYS CFX 12.1 and Tecplot was used for post processing the data after the simulations. The time step size used for convergence of the solution used for the steady state solution was automatic time step with a timescale factor of 5. Information of size of the domain, the flow physics and boundary condition settings are used by CFX solver to calculate the value of physical time step size by itself (CFX-solver guide). Convergence of the simulation is assumed when the residuals of mass, momentum and turbulence reaches to less than $1 \times 10^{-5}$ with a minimum of three coefficient loop iteration for each time step. Residuals of momentum equations were showing oscillatory behavior but residuals of moment and mass flow rate were steady after 200 iterations in most of the cases. Total time to reach the convergence took about 6 to 15 hours.

The geometry of the turbine was designed by Mechanical Solution Inc. using Blade modeler. The design has been explained in the report “Horizontal Kaplan Turbine design and CFD analysis”. Chapter 4 deals with geometric model development and the properties of the turbine components.

# CHAPTER 4 MODEL DEVELOPEMENT

The geometry of the Kaplan turbine consists of shrouded runner, stationary wicket gates and a draft tube. The geometry was designed by Mechanical Solution Inc. using ANSYS Blade Modeler. Number of wickets has been set to nine in a full row such that there would be minimal flow deviation off the gate. The wicket gates have been designed based upon the shape of modified NACA airfoil with constant cross section and linear variation of vane angle from leading edge to the trailing edge. Three runner blades were designed in a full row with blade shape based on modified NACA airfoil with linear vane angle from leading edge to trailing edge. The properties of the wicket gates and runner blade are given in table below:

**Table 4.1 Wicket gates properties**

| **Design properties** | **Value** |
|---|---|
| Tip radius | 63.228 in |
| Chord length | 23.084 in |
| Stagger angle | 9.1 deg |
| Exit vane angle | 72 deg |
| Solidity | 1.476 |
| Hub/Tip radius ratio | 0.4 |
| Max thickness and camber line length ratio | 0.175 |

**Table 4.2 Runner blade properties**

| **Design properties** | **value** |
|---|---|
| Tip radius | 63.228 in |
| Hub/tip radius ratio | 0.4 |
| Runner hub: | |
| Chord length | 32.368 in |
| Stagger angle | -31.3° |
| Exit vane angle | 62.5° |
| Solidity | 1.172 |
| Max thickness/camberline length ratio | 0.2 |
| Runner shroud: | |
| Chord length | 58.716 in |
| Stagger angle | -69° |
| Exit vane angle | 17.5° |
| Solidity | 0.886 |
| Max thickness/camberline length ratio | 0.075 |

The draft tube was first designed to be a straight cylindrical tube but later it was modified to a conical shaped according to Paul Roos, Technical Director of ATS, so that there is smooth transition for the flow at the outlet and a minimum amount of loss is maintained. For numerical analysis of this turbine, the geometry for mesh development was taken from pressure location at Tap A to Tap D as shown in the schematic diagram in Figure 6.1. The inlet pipe is 20 inches long connected to the entry bell of the turbine

with conical shaped draft tube. There is a small variation in the inlet diameter of the cylinder. The experiment prototype has the diameter of 11.89 inches whereas the CFD model has the inlet diameter of 10.72 inches.

Numerical simulation requires discretizing the fluid domain into finite volume to perform partial differential equations to get the required solution. The accuracy of the solution depends on the quality of the mesh so the aspect ratio; minimum and maximum angle of the cell has to be carefully checked to get the desirable solution. Following chapter deals with all procedures regarding generation of meshes.

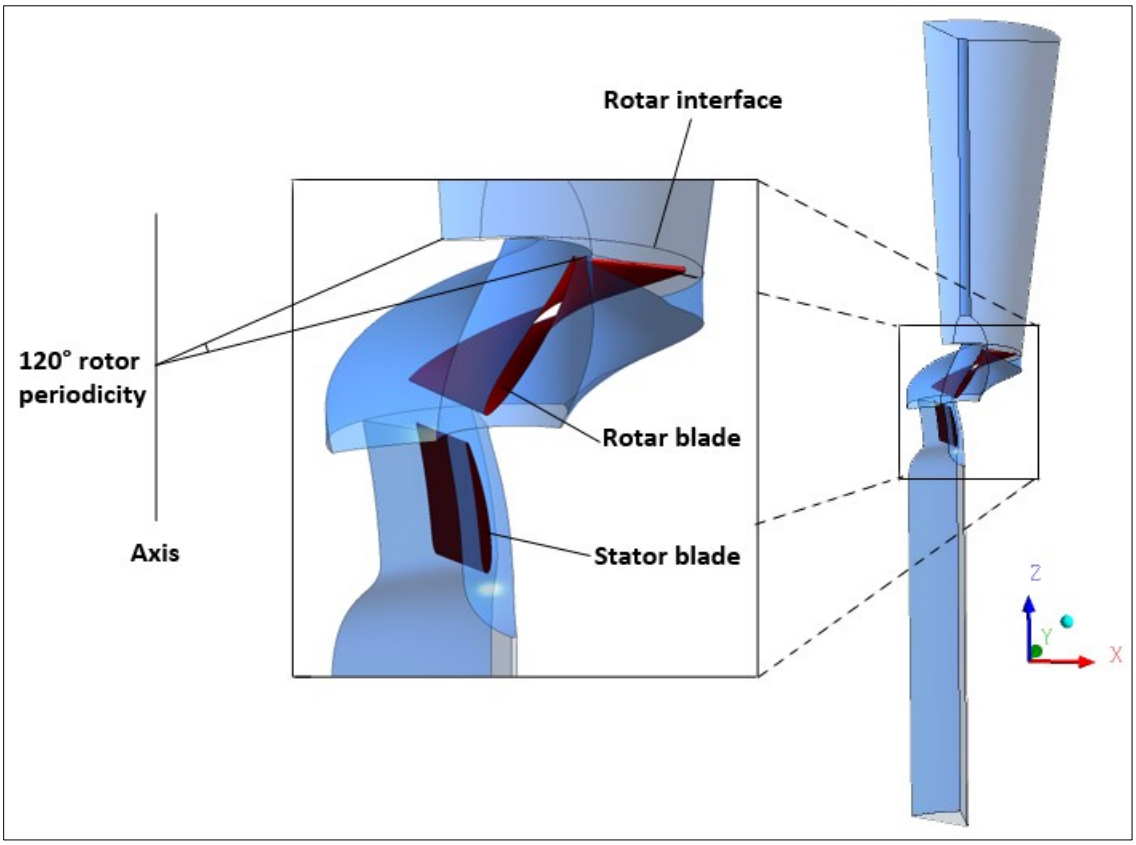


**Figure 4.1 Rotor and stator interface with pitch ratio unity**

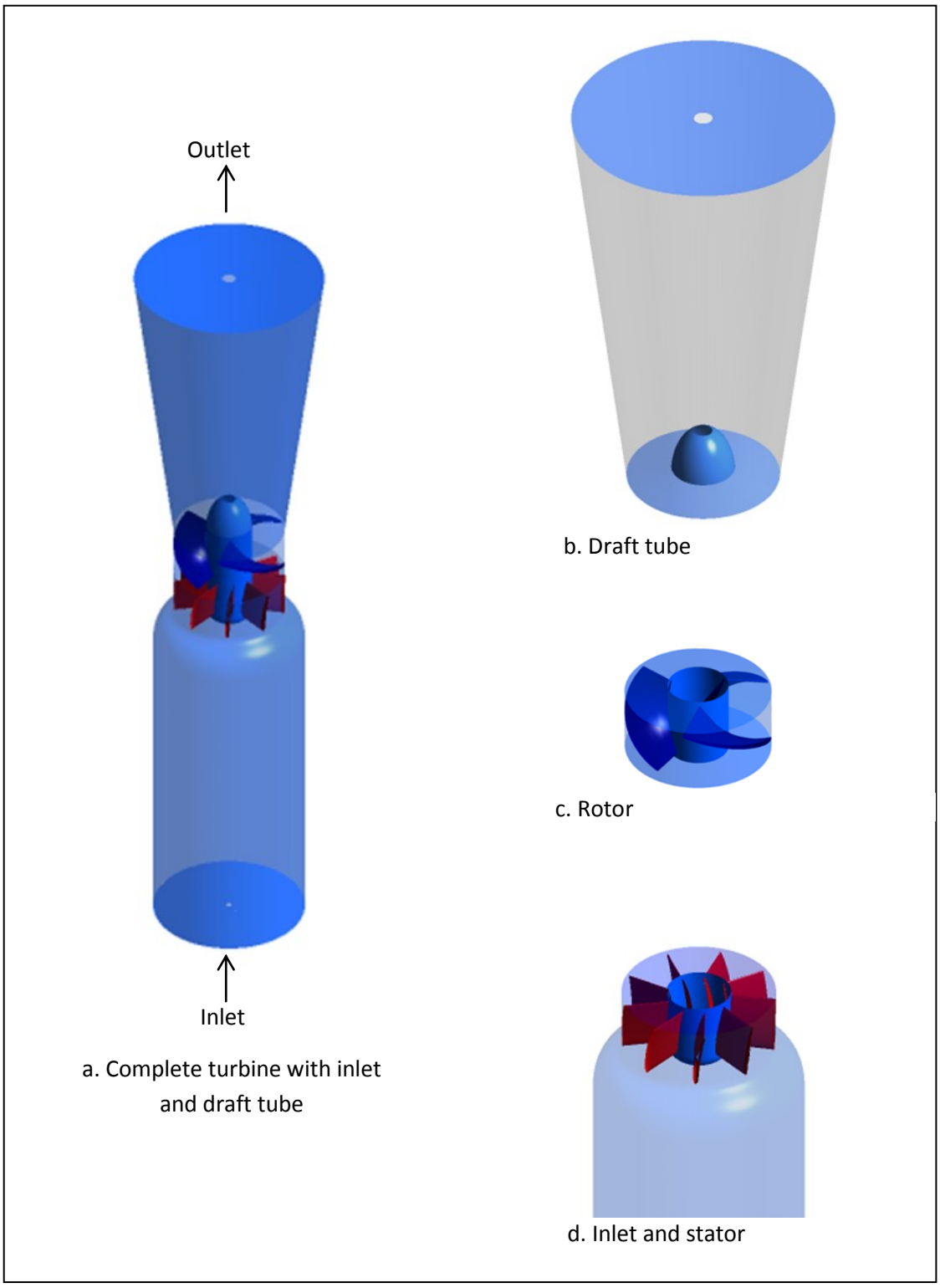


**Figure 4.2 Separate views of the turbine components**

# CHAPTER 5 MESH DEVELOPMENT

The geometry that well represents the actual flow phenomena is developed for CFD simulation. Control volumes are developed by a meshing tool to represent fluid flowing in the object on which flow governing equations are solved. The geometry of the turbine is complex, so generally the whole geometry is divided into components to generate the mesh and these components are later joined together by creating interfaces while preprocessing. For simplicity, this turbine as well is divided into three components: Inlet pipe with stator blades, rotor domain and a draft tube. The inlet and the draft tube of the turbine were meshed in Gridgen. For the rotor component it was difficult and time consuming to develop the mesh in Gridgen considering the required aspect ratio and skewness of the rotor blade. Hence, ANSYS Turbogrid was employed to generate the grid for rotor component regarding the required criteria for mesh generation.

As the turbine possesses rotational periodicity, part of geometry of the total domain was considered for simulation. Only one segment of runner and stator blade was considered out of 3 runner and 9 stator blades of the complete turbine for the simulation. As a passage of turbine simulation will give same flow results as of entire machine, consideration of whole turbine would only cause increases in computational time in the effort. Hence a part of the geometry is considered to reduce computational time.

3D structured mesh of hexahedral cells is generated. Total number of nodes in the passage is 1.3 million. Number of nodes was referenced from the mesh developed by Mechanical Solution Inc. They simulated for the full scale design of the turbine to obtain the efficiency of the turbine at three operating heads. The only difference between the

full scale design and the prototype was the draft tube shape which was straight in full scale design and conical in the prototype (Ivashchenko, Bennett. 2010). The prototype simulation consisted of the inlet pipe as well so the number of nodes was increased to 1.3 million. Number of nodes increased did not bring change in the value of torque. Hence, this number of nodes was accepted for which the flow parameters were independent of.

The $Y^+$ value is maintained to be lower than 200 in almost all locations of the domain which are acceptable for automatic wall treatment for the boundary layer for shear stress transport model. But at some locations around the hub at the upstream of the stator blade, $Y^+$ is around 1500.

### 5.1 Inlet guide vane model

The inlet and guide vane model was completed in Gridgen V15. In order to produce realistic flow, an inlet pipe of length 20 inch was also modeled. Moreover, the pressure at Tap A was located upstream of the entry bell to the stator which added benefit to use the experimental values for inlet. The average angle of the cell is 82° and the $Y^+$ value is less than 50. In some location $Y^+$ value has been found to be 300 which were difficult to avoid due to complex geometry of the turbine. In order to make a refined mesh around the stator blade, a separate domain was made close to the stator blade with number of nodes 15. Number of nodes used in overall domain is 768240. The number of nodes near the interface to the rotor blade is increased so that the flow variables are properly captured as they flow from non-rotating to rotating component. The complexity in getting a good quality mesh required change in the geometry of the

fluid flow while creating in Gridgen. A part of the fluid flowing volume was made wall. $Y^+$ values at some locations were above 1500 where proper mesh generation was difficult with Gridgen on geometry of such complexity.

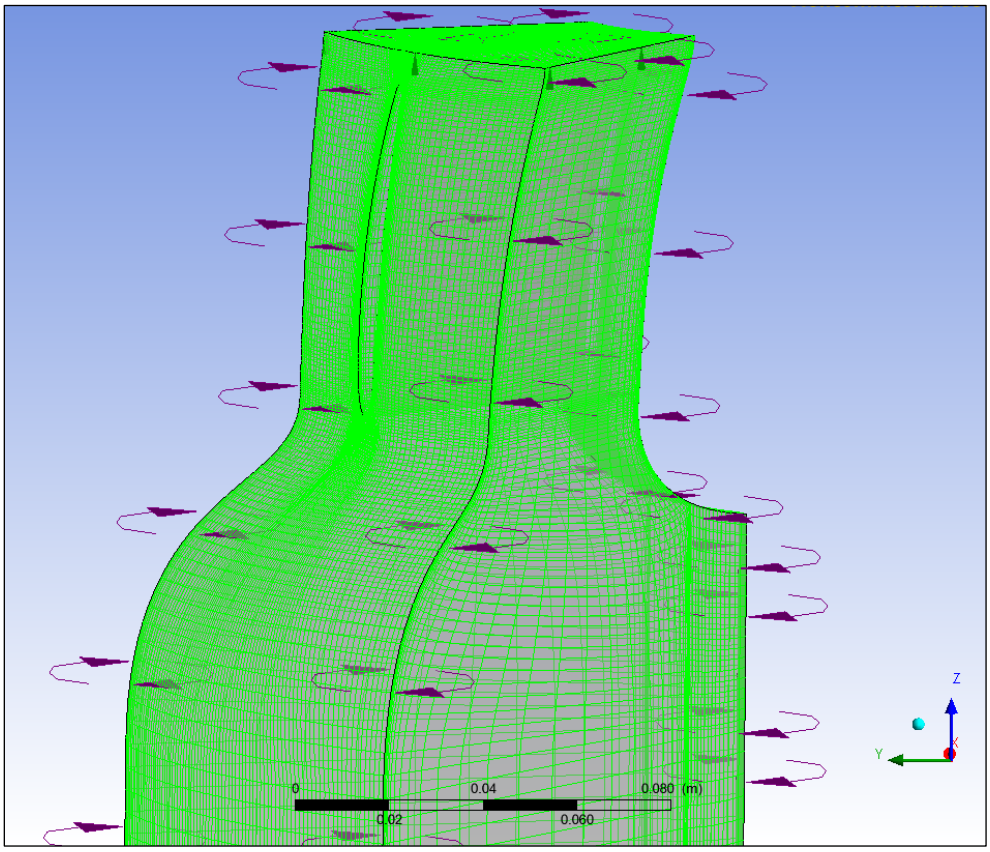


**Figure 5.1 Stator mesh model**

### 5.2 Rotor model

Due to the complexity in geometry of the rotor component, it was meshed in ANSYS Turbogrid to create high quality hexahedral mesh to account for complex flow problems. The .curve file for turbogrid was produced by importing the grids from the geometry in Gridgen. Sufficient numbers of nodes were placed to maintain the shape of

the rotor blade. An O grid was used for the mesh generation. Number of nodes used was 260220. The $Y^+$ values were checked in CFX post with minimum and maximum value ranging from 2 to 60 which is appropriate for shear stress transport model. No tip clearance was provided as the runner blade is attached with the shroud and rotates with same rotational speed as the runner blade. The boundary condition for blade shroud and hub is considered as walls.

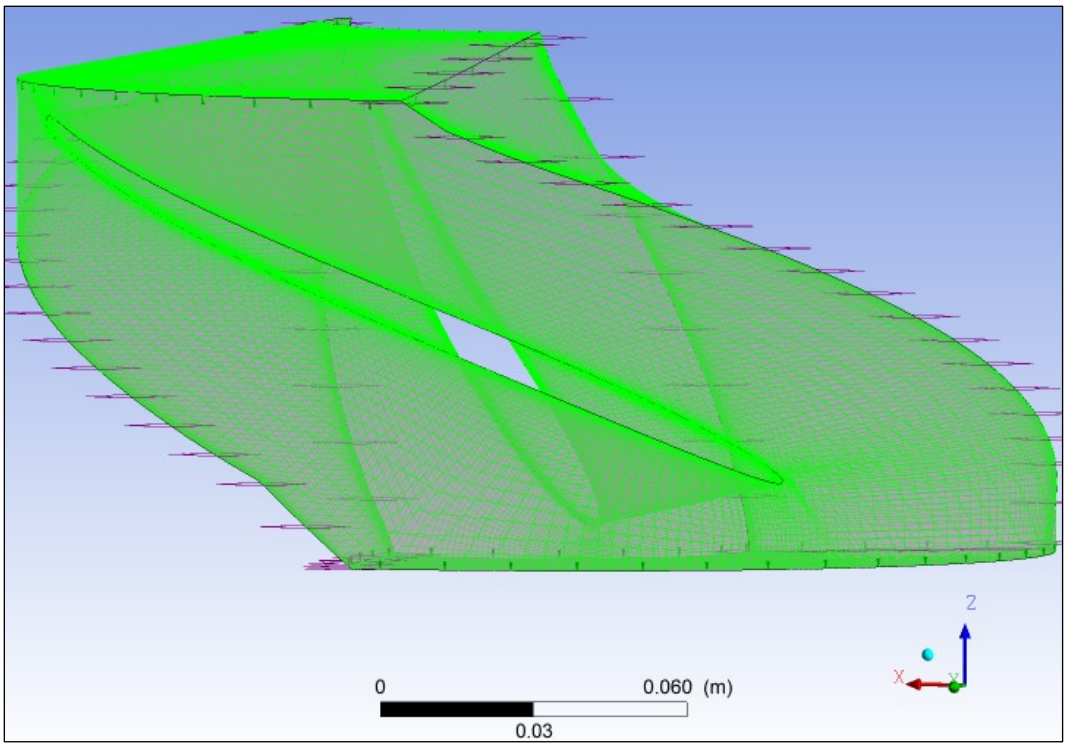


**Figure 5.2 Rotor model mesh**

### 5.3 Draft tube

A conical draft tube was designed to minimize recirculation losses and smooth transition of the flow through the outlet of the rotor domain. Number of nodes used in this draft

tube domain is 308000. $Y^+$ value of the draft tube is between 8 –100. The section of a draft tube is considered as a wall. The reason for making this is to develop high quality mesh with less skewed angles at the tip of the hub. This would not have much effect on the hydrodynamics of the turbine. Table 5.1 shows the number of nodes, elements and its type for all three domains.

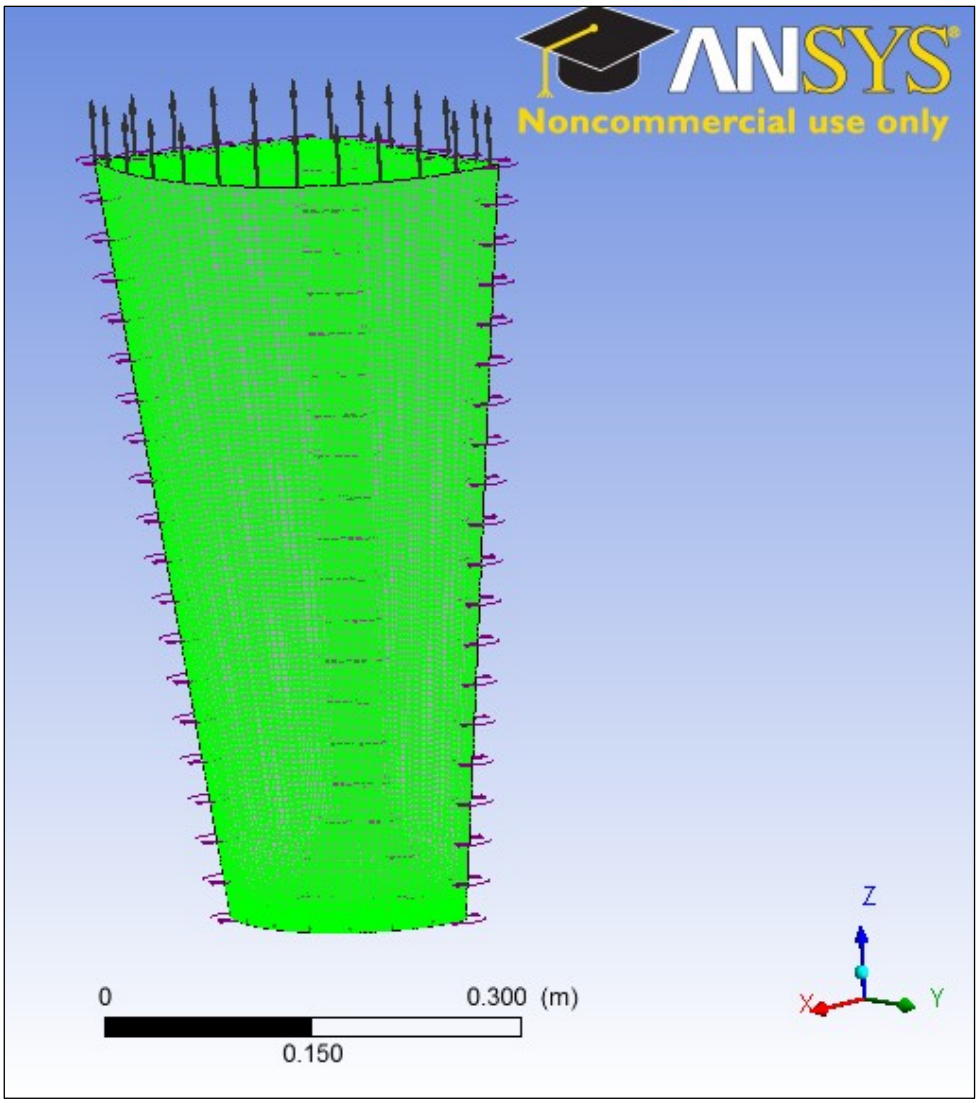


**Figure 5.3 Draft tube mesh**

**Table 5.1 Summary of mesh data**

| Component | No. of nodes | No. of elements | Type of element |
|---|---|---|---|
| Inlet and stator | 768240 | 2758722 | Hexahedral |
| Rotor | 260220 | 716800 | Hexahedral |
| Draft tube | 308000 | 290472 | Hexahedral |

Next chapter deals with brief description about how the experiment of the prototype horizontal Kaplan turbine was conducted in the Hydraulic Annex.

# CHAPTER 6 EXPERIMENTAL FLUID DYNAMICS

Experimental fluid dynamics of the prototype turbine was carried out at the IIHR's Hydraulic Annex # 2 to perform hydrodynamic, electrical and mechanical performance of the turbine system. As the impeller and generator behave as a single unit, the rotational motion transfers the mechanical energy into electrical energy through the magnetic field that is developed by the permanent magnets around the periphery of the turbine. A large sump at the facility made the experiment to perform on a circulating type of closed loop which made it possible to carry out ample numbers of tests.

The prototype was designed by MSI and the construction of prototype and test stand was done by Alcar Design and Manufacturing Inc. of Keokuk, Iowa.

The objective of the experiment was to construct the performance map for hydrodynamic, electrical and mechanical study. The input parameters in the experiment were the discharge and torque on the machine. Pressure at tap C was set to atmospheric pressure throughout the entire test so that the data could be compared.

The turbine is a scaled down model of 1:7.828 of the full scaled design by MSI. The test stand consists of a cylindrical pipe, a bell shaped inlet, a stator section with nine blades, rotor section with three blades and a conical draft tube. The periphery of the shroud of a rotor is covered by permanent magnets. When discharge is run through the inlet, the rotor blade rotates which develops magnetic field to produce electricity. The transducers are ported at the periphery of the system at four different locations. Following schematic diagram shows the location of the pressure taps. A single port is placed at location A, at the inlet and at D, single dial pressure gage at the exit in a draft

tube. Four ports are located at B just upstream of the stator blade and at C just downstream of the rotor blade and circumferential average of the static pressure is determined. The flow is in the z axis as shown in the schematic diagram in Figure 6.1.

The details of the experiment have been explained in the report "Laboratory tests of the ATS integrated hydroelectric turbine/generator prototype". Next chapter presents the results from CFD simulation and results from experiment and comparison is made on the basis of power, torque and discharge.

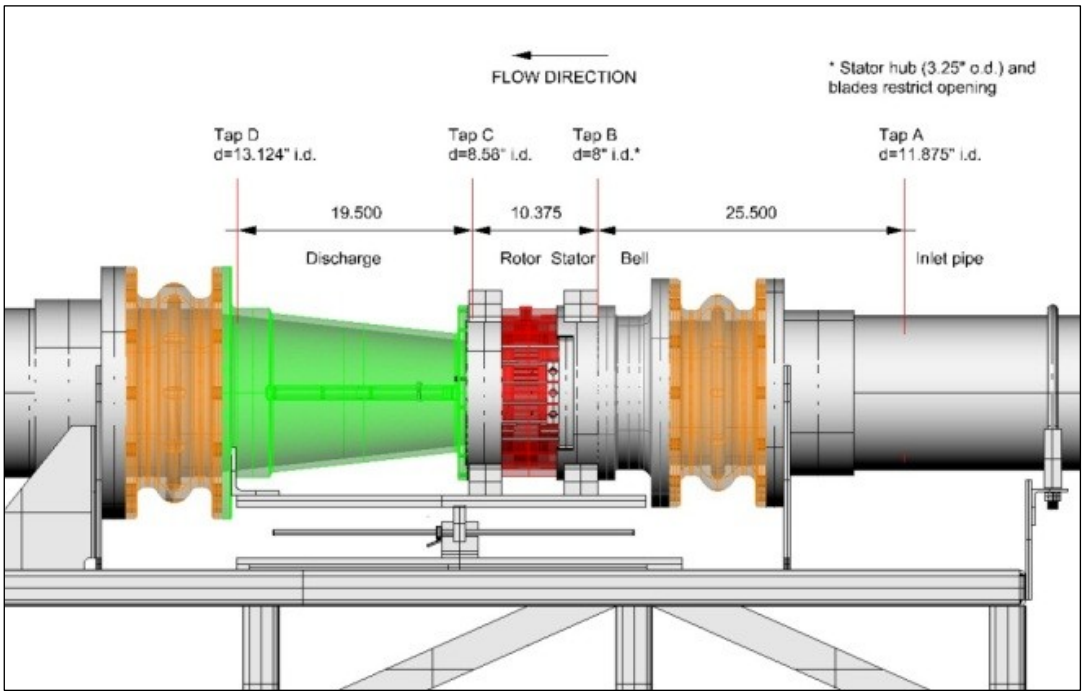


**Figure 6.1 Schematic diagram of the ATS turbine on its test stand**

Source: Longo et al, laboratory test of the ATS integrated hydroelectric turbine/generator prototype, 2012

# CHAPTER 7 RESULTS AND DISCUSSION

The input variables for the CFD analysis are used from the experimental data in order to match the output of the simulation with the experiment. The objective of the study is to plot the performance curve of the turbine for different head and compare the result obtained from the experiment.

As discussed earlier the boundary condition for the simulation is chosen as total pressure inlet and static pressure outlet.

Total pressure = static pressure +dynamic pressure

Static pressure is given by the pressure measured by the transducers while dynamic pressure is calculated with the discharge obtained from the experiment. With continuity equation, velocity in the pipe is calculated to obtain the dynamic pressure.

Five experimental cases are taken for 30 feet of head to plot the curve of RPM vs. power and discharge vs. power. The power calculated from CFX is obtained from the torque developed on the rotor blades. The torque acting on a runner is the resultant of pressure and viscous moments. It is the surface integral of cross product of stress tensor and radius vector.

$$T = \int (r \times (\tau . n) dS) . a \ldots\ldots (7.1)$$

Output power of the turbine is calculated by the following equation

$$P = nT\omega \ldots\ldots (7.2)$$

Here,

P = mechanical power developed by the turbine (watts)

N= number of blades

T= Torque developed on the blade due to moment in Z axis (N-m)

ω = angular speed (radian) (Jain et al., 2010)

Since one blade row is used in the simulation, torque produced will be for one blade only. Total torque acting on a runner is calculated by multiplying torque by total number of blades in a turbine.

Table 7.1 shows the diameter of the pipe at tap location of the prototype and Table 7.2 shows pipe diameter of the geometry used for the simulation. The diameter of the pipe for tap located at A differs by 1 inch. This variation could lead to a boundary condition that is different from the experiment. So adjustment in the pressure head is made by decreasing the static head by the same value dynamic pressure has increased with the increase of velocity. This is one of the limitation of this research which should be considered for the future works.

**Table 7.1 Diameter of pipe at tap location for EFD**

| SN | Diameter(in) | Area(sqft) |
|---|---|---|
| Tap A | 11.89 | 0.77 |
| Tap B | 8.00 | 0.35 |
| Tap C | 8.61 | 0.40 |
| Tap D | 13.75 | 1.03 |

**Table 7.2 Diameter of the pipe at tap location for CFD**

| SN | Diameter (in) | Area (sqft) |
|---|---|---|
| Tap A | 10.72 | 0.63 |
| Tap B | 8.00 | 0.35 |
| Tap C | 8.61 | 0.40 |
| Tap D | 13.75 | 1.03 |

The simulations were conducted for 30 feet of head which is the net head difference between the tap location B and C of the turbine. Six cases for 30 feet of head from the experiment were run in CFX with boundary conditions as total pressure at inlet and static pressure at outlet. The data were extracted from the cases from the experiment which were the interpolated data from number of measurements run on the physical model (Longo et al., 2012). Table 7.3 shows the input data in CFX for the six cases for 30 feet of head. The static pressure at tap A and D, volumetric flow rate which is used to calculate dynamic pressure and RPM are used as inputs for the simulation.

The power developed by the turbine is directly proportional to the net head developed between inlet and outlet of the turbine which can be expressed by the following equation.

$$P = \rho g Q H \ldots\ldots (7.3)$$

As mentioned earlier, there is a variation in geometry of the inlet pipe in between the CFD model and the prototype tested in the lab. The inlet of the CFD geometry is an

inch shorter than the prototype. Total pressure at the inlet is given by static head and dynamic head.

**Table 7.3 Input parameter for CFX simulation**

| Simulation | N(RPM) | Discharge(cfs) | Total inlet pressure(ft) | Outlet static pressure pD (ft) |
|---|---|---|---|---|
| S1 | 1333 | 8.08 | 41.69 | 4.46 |
| S2 | 1827 | 9.06 | 44.97 | 4.59 |
| S3 | 2259 | 9.88 | 47.98 | 4.19 |
| S4 | 2730 | 11.43 | 53.87 | 7.85 |
| S5 | 2866 | 12.1 | 57.01 | 9.42 |
| S6 | 3350 | 13.45 | 63.93 | 16.56 |

With the change in inlet area of the pipe, discharge of the fluid will vary, which will change the dynamic head at the inlet. Hence, in order to create similar condition as in the prototype, static head is modified with the change in the dynamic head created by the variation in the inlet dimension in order to match the total head with that of the experiment. The available data constant head of 30 feet is used to compare the power produced by the experiment with the CFD simulation. For this investigation, the whole regime of the curve is considered for simulation including the peak point where the turbine exhibits best efficiency with maximum power for given head. Six cases were run

with the RPM values ranging from 1333 to 3350 RPM and with the discharge of 8 cfs to 13.45 cfs.

With the given input values, equations of mass and momentum are solved numerically on discretized volume and discharge and torque on a blade is provided as output by the solver. With the torque produced on the blade, mechanical power produced by the turbine can be calculated with the equation 7.2.

Head developed by the turbine can also be obtained by applying Bernoulli's equation at tap B and C with following equation.

$$\frac{P_B}{\gamma} + \frac{{V_B}^2}{2g} + Z_B = \frac{P_C}{\gamma} + \frac{{V_C}^2}{2g} + Z_c + H_l + H_T \ldots\ldots (7.4)$$

As the turbine is a power producing machine, the head developed is positive. Through this equation, head developed between the rotor and stator is calculated. As the head loss within the turbine is not known from the simulation, the head developed through the above equation includes the head loss as well.Table 7.5 shows the pressure and velocity head developed at the four tap locations from the CFD simulation and net head developed between the Tap B and C. Pressure head at A has been modified so that the total head which is the sum of static pressure head and dynamic head in the simulation is the same as that in the experiment. Table 7.4 shows the discharge at inlet and outlet, torque developed on the rotor blade as the output from CFD. Power was calculated with total torque developed on three rotor blades. Mechanical power was also calculated from the net head developed between Tap B and C by applying the energy equation at those two points. Similarly, Table 7.6 shows pressure, velocity head at the tap locations B and C as obtained from the experiment and net energy between the Tap B and C. The

pressure head was calculated from the pressure transducer and velocity head was calculated by the continuity equation with the discharge measured from the experiment. Comparison of the CFD analysis is done on the basis of power developed in the turbine.

**Table 7.4 Output from CFX simulation**

| Simulations | N(RPM) | Discharge at inlet CFD (cfs) | Discharge at outlet CFD (cfs) | Total torque (Nm) | Power CFD Kw |
|---|---|---|---|---|---|
| S1 | 1333 | 7.26 | 7.22 | 118.4 | 13.23 |
| S2 | 1827 | 8.07 | 8.03 | 107.2 | 16.42 |
| S3 | 2259 | 9.02 | 8.97 | 105.9 | 20.04 |
| S4 | 2730 | 10.07 | 10.00 | 92.3 | 21.13 |
| S5 | 2866 | 10.42 | 10.36 | 92.6 | 22.23 |
| S6 | 3350 | 11.45 | 11.39 | 76.5 | 21.48 |

Figure 7.1 shows comparison of power vs. RPM from experiment and CFD simulation. The mechanical power is calculated from CFD with the moment developed on the blades about the Z axis. The power obtained from the experiment was calculated as electrical power, mechanical power was then calculated assuming that the electrical efficiency is about 80%. In Figure 7.1 we can observe that there is discrepancy in the value between CFD and experiment at partial load and at overload condition. But at the peak load condition the CFD value almost matches with the experimental value.

In Figure 7.2 the comparison is made between curves developed from experiment and the power developed from the head calculated by applying Bernoulli's equation between the Tap B and C. The Green curve represents the data extracted from the experiment and red and blue curve represents the power developed from the energy equation at the Tap B and D from CFD simulation, with considering the losses and without considering losses respectively. With the increase in RPM, volumetric discharge in the turbine increases. As we know that power is directly proportional to the discharge and head, at constant head power increases with the increase in discharge but after optimum power, it starts decreasing which is due to various types of losses in the turbine. Power should increase with increase in RPM and discharge whereas in reality the power decreases after it has reached its optimum value. But, from Figure 7.1 we see that the power at overload condition does not follow the trend of the experiment. This might be due to the losses that have not been incorporated. If we consider the losses from the experiment on the simulation, the curve follows the trend of the experimental characteristic curve.From the literature, we have found that the numerical simulation provides accurate results for the optimum condition of a turbine with errors at regimes away from the best efficiency point (Gagnon and Deschênes., 2007).Another set of simulations was run for the cases with peak load condition for head between 20 ft. to 48 ft. to compare with the EFD results. The electrical efficiency was assumed to be 80% for all of the cases. Performance curve was plotted for different head from the simulation data and the plot was overlaid with experimental data to make a comparison between variables power, discharge and torque. Figure 7.3, 7.4 and 7.5 shows the performance curve for variables torque, discharge and power, respectively, for peak load conditions from head varying from 20 feet to 50 feet.

**Table 7.5 Pressure and velocity head from simulation at four differed tap from simulation**

| Tap | X (ft) | Simulation 1 | | Simulation 2 | | Simulation 3 | | Simulation 4 | | Simulation 5 | | Simulation 6 | |
|---|---|---|---|---|---|---|---|---|---|---|---|---|---|
| | | Pressure head (ft) | Vel head (ft) | Pressure head (ft) | Vel head (ft) | Pressure head (ft) | Vel head (ft) | Pressure head (ft) | Vel head (ft) | Pressure head (ft) | Vel head (ft) | Pressure head (ft) | Vel head (ft) |
| A | 0 | 39.1 | 2.09 | 41.72 | 2.58 | 44.13 | 3.22 | 48.71 | 4.02 | 51.23 | 4.3 | 56.78 | 5.19 |
| B | 2.17 | 27.91 | 10.2 | 27.78 | 12.67 | 26.57 | 15.88 | 27.25 | 19.88 | 28.47 | 21.34 | 29.26 | 25.89 |
| C | 3 | -0.91 | 10.29 | 5.9 | 5.16 | 6.54 | 4.62 | 8.49 | 5.95 | 9.52 | 6.59 | 11.86 | 10.4 |
| D | 4.62 | 4.46 | 0.76 | 4.59 | 0.94 | 4.19 | 1.18 | 7.85 | 1.46 | 9.42 | 1.57 | 16.56 | 1.9 |
| Δ BC | | 28.72 | | 29.38 | | 31.29 | | 32.69 | | 33.69 | | 32.89 | |

**Table 7.6 Pressure and velocity head at four differed tap location from experiment**

| Tap | X (ft) | Experiment 1 | | Experiment 2 | | Experiment 3 | | Experiment 4 | | Experiment 5 | | Experiment 6 | |
|---|---|---|---|---|---|---|---|---|---|---|---|---|---|
| | | Pressure head (ft) | Vel head (ft) | Pressure head (ft) | Vel head (ft) | Pressure head (ft) | Vel head (ft) | Pressure head (ft) | Vel head (ft) | Pressure head (ft) | Vel head (ft) | Pressure head (ft) | Vel head (ft) |
| A | 0 | 39.98 | 1.71 | 42.82 | 2.15 | 45.44 | 2.55 | 50.46 | 3.42 | 53.19 | 3.83 | 59.2 | 4.73 |
| B | 2.17 | 27.8 | 8.34 | 27.23 | 10.48 | 26.8 | 12.46 | 25.95 | 16.69 | 25.44 | 18.69 | 24.29 | 23.08 |
| C | 3 | -0.07 | 6.21 | -0.09 | 7.8 | -0.02 | 9.27 | 0.21 | 12.42 | 0.2 | 13.91 | 0.18 | 17.18 |
| D | 4.62 | 4.46 | 0.96 | 4.59 | 1.2 | 4.19 | 1.43 | 7.85 | 1.91 | 9.42 | 2.14 | 16.56 | 2.65 |

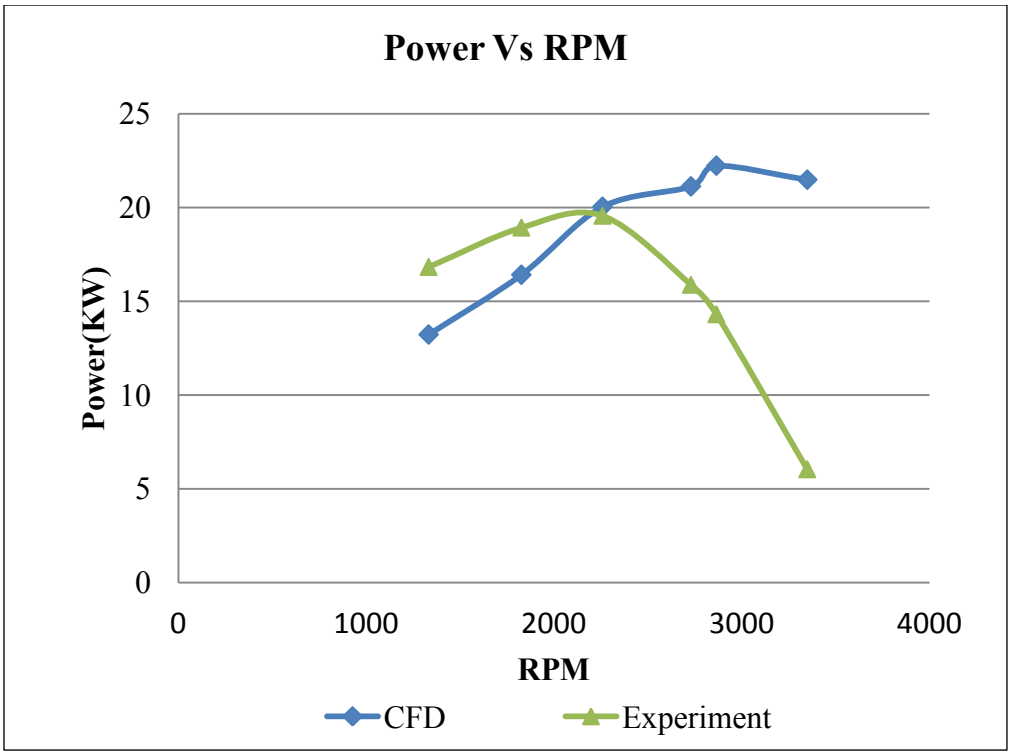


**Figure 7.1 Power vs. RPM from simulation and experiment**

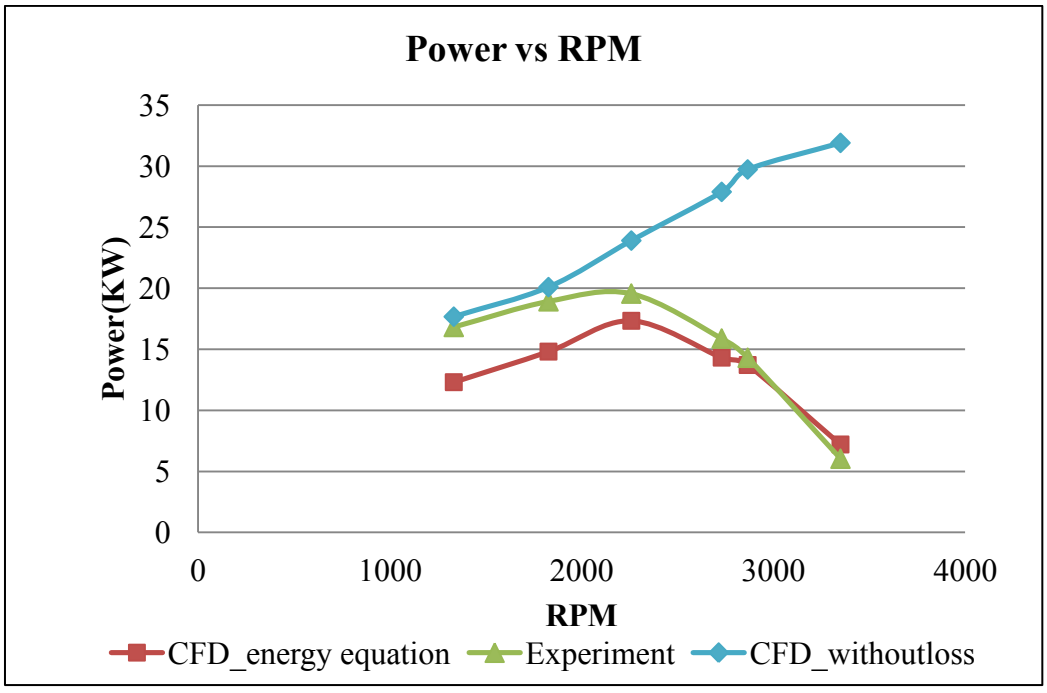


**Figure 7.2 Power vs. RPM**

Table 7.7 shows error in the values obtained from CFD and experiment for torque, discharge and power. For power vs. head, we can see the CFD values are near to the experiment for 29.71ft, 31.43ft, 33.46ft, and 35.77ft with discrepancies of 8.88%, 7.33%, 1.27%, and 2.77%, respectively. For head below 29.71ft, power from CFD is below the experiment and for head above 35.77ft, CFD power is above the experiment. In case of discharge vs. head, for the entire peak load condition the discrepancy is below 9% though they follow the same curve pattern as obtained from experiment. The discharge in CFD is larger than the discharge in actual experiment. This might be due to variation in geometry of the inlet section. Fluctuation in torque value increases with the increase in head up to 50% of the experimental value. Variation in the value of power torque and discharge can be due to the variation of geometry of prototype and CFD model.

The differences in the efficiencies between experimental and simulation at off load conditions might be due to errors in discretization of governing equation, losses not fully accounted for, and might be due to considering only a part of a geometry (Prasad Vishnu et al., 2009). As the cases were run with steady state analysis with stage averaging, fluxes are circumferentially averaged out when they move from rotating to non-rotating frame. When these are averaged out, losses are not cooperated precisely. When flow rate is varied, flow tends to be unsteady and this unsteadiness increases if the operation point is away from the best efficiency point (Gagnon and Deschênes., 2007).

The plots also show four cases run by Mechanical Solution Inc. for a head of 15 ft., 20ft, 38 ft and 55 ft. The results obtained from their simulation also show differences from the experimental value.

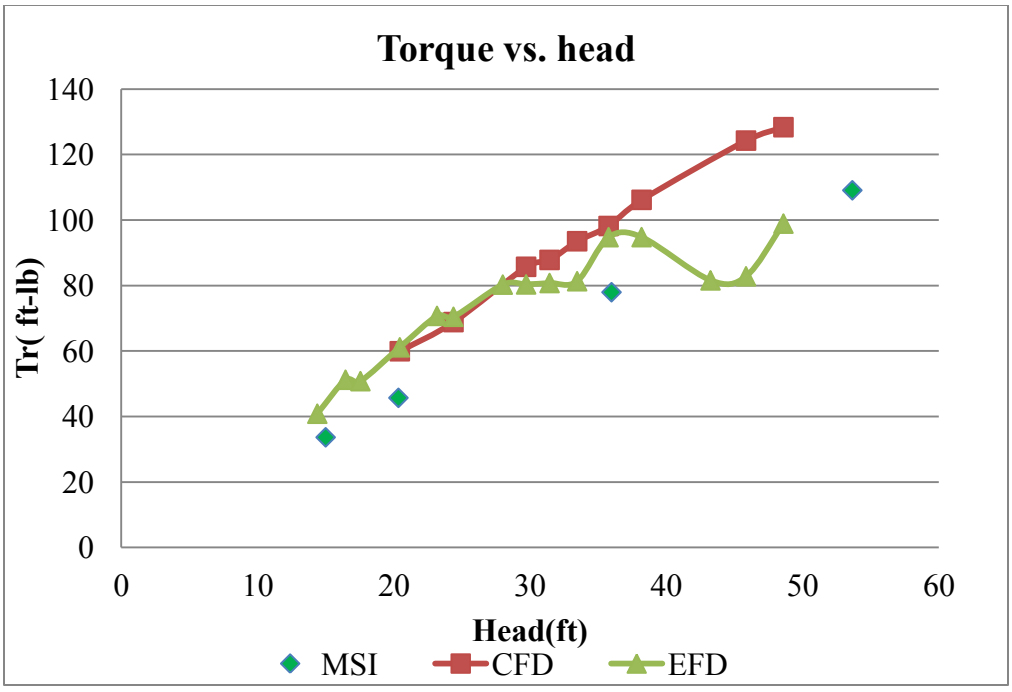


**Figure 7.3 Torque vs. RPM for peak load condition**

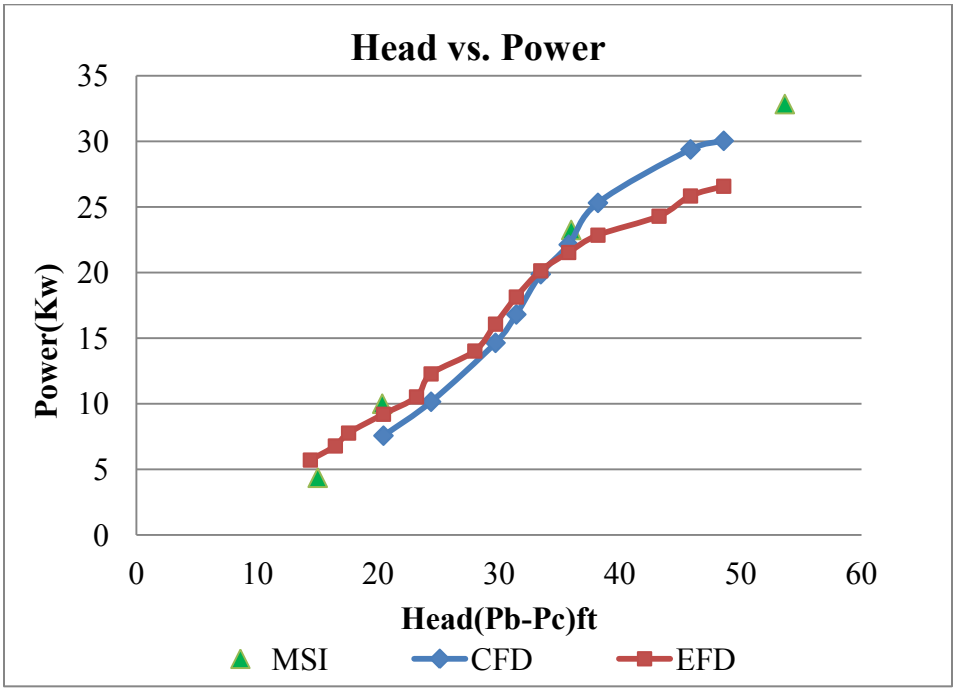


**Figure 7.4 Power vs. RPM for peak load condition**

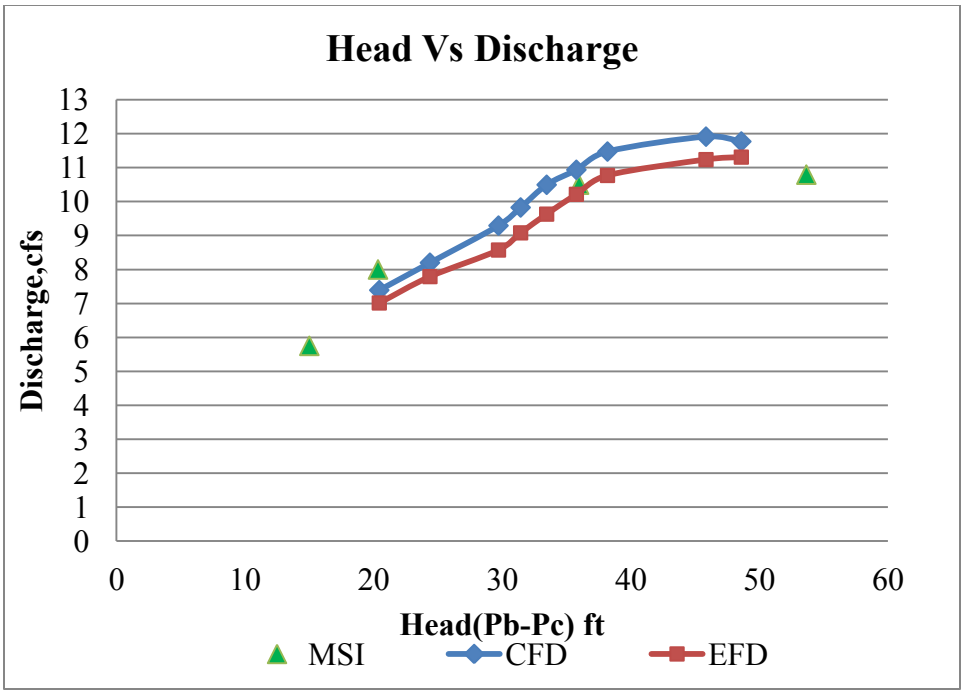


**Figure 7.5 Discharge vs. RPM for peak load condition**

Figure 7.6 shows the slice of the passage of the runner at the mid span in a 3D view. This 3D plane is projected on a 2D plane to view the pressure contours and velocity streamlines more clearly. Figure 7.6 is shown in cartesian coordinates. Pressure contours and velocity streamlines at the mid span of the runner blade is shown in Figure 7.8 and 7.9. Only one runner blade is shown in the diagram as similar flow exists in all the passages due to periodicity.Figure 7.7 shows the sliced surface of the blade in a 2D plane showing leading and trailing edge and pressure and suction side. As Gagnon stated that the flow parameters of experimental results and the simulation is similar for the cases of operating regimes near to the best efficient point, three operating regimes are selected from characteristic curve developed for 30 feet of head. Figure 7.8 and 7.9 shows the pressure contour and velocity streamlines at the mid span of the runner blade for three operating regimes for 30 feet of head.

**Table 7.7 Output from the simulation at peak load conditions.**

| Head(B-C) | RPM | Torque (CFD) Ft-lb | Discharge at inlet (CFD) Cfs | Discharge at outlet (CFD)cfs | Power (CFD) kw | Power (EFD) Kw | Discharge (EFD) cfs | %error in power | %error in Discharge | %error in Torque |
|---|---|---|---|---|---|---|---|---|---|---|
| 20.44 | 1110 | 59.9 | 7.39 | 7.35 | 7.55 | 9.19 | 7.01 | -17.78 | 4.75 | -1.96 |
| 24.38 | 1297 | 68.8 | 8.20 | 8.15 | 10.14 | 12.26 | 7.79 | -17.30 | 4.63 | -2.30 |
| 29.71 | 1503 | 85.7 | 9.29 | 9.24 | 14.63 | 16.06 | 8.57 | -8.88 | 7.75 | 6.69 |
| 31.43 | 1684 | 87.8 | 9.83 | 9.77 | 16.80 | 18.13 | 9.08 | -7.33 | 7.60 | 8.74 |
| 33.46 | 1870 | 93.5 | 10.49 | 10.43 | 19.87 | 20.12 | 9.63 | -1.27 | 8.35 | 15.02 |
| 35.77 | 1984 | 98.1 | 10.94 | 10.87 | 22.12 | 21.52 | 10.21 | 2.77 | 6.45 | 3.59 |
| 38.19 | 2099 | 106.1 | 11.47 | 11.41 | 25.31 | 22.84 | 10.77 | 10.79 | 5.92 | 12.01 |
| 45.85 | 2082 | 124.2 | 11.91 | 11.84 | 29.38 | 25.83 | 11.24 | 13.74 | 5.40 | 50.04 |
| 48.60 | 2060 | 128.3 | 11.77 | 11.89 | 30.04 | 26.75 | 11.31 | 13.04 | 5.15 | 29.77 |

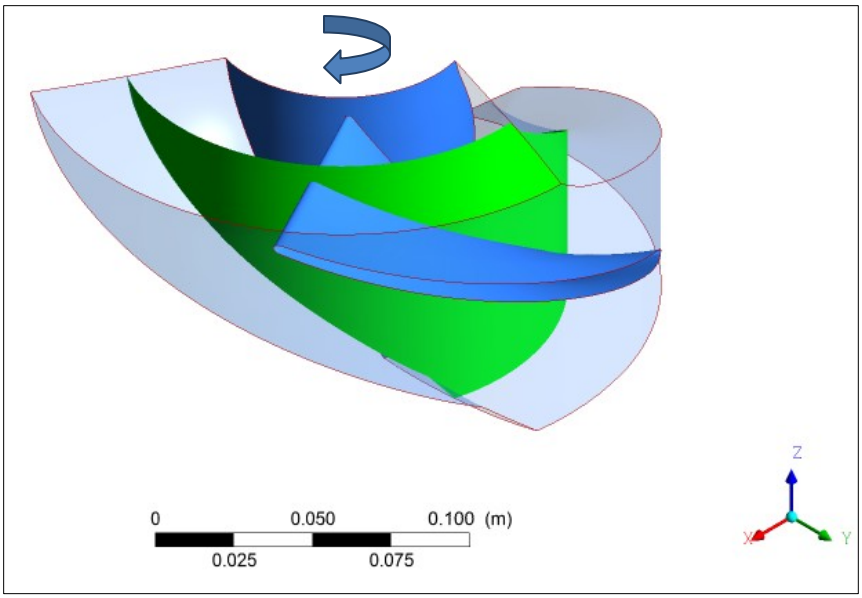


**Figure 7.6 Isometric view of one passage of rotor showing a surface at the mid span of the blade**

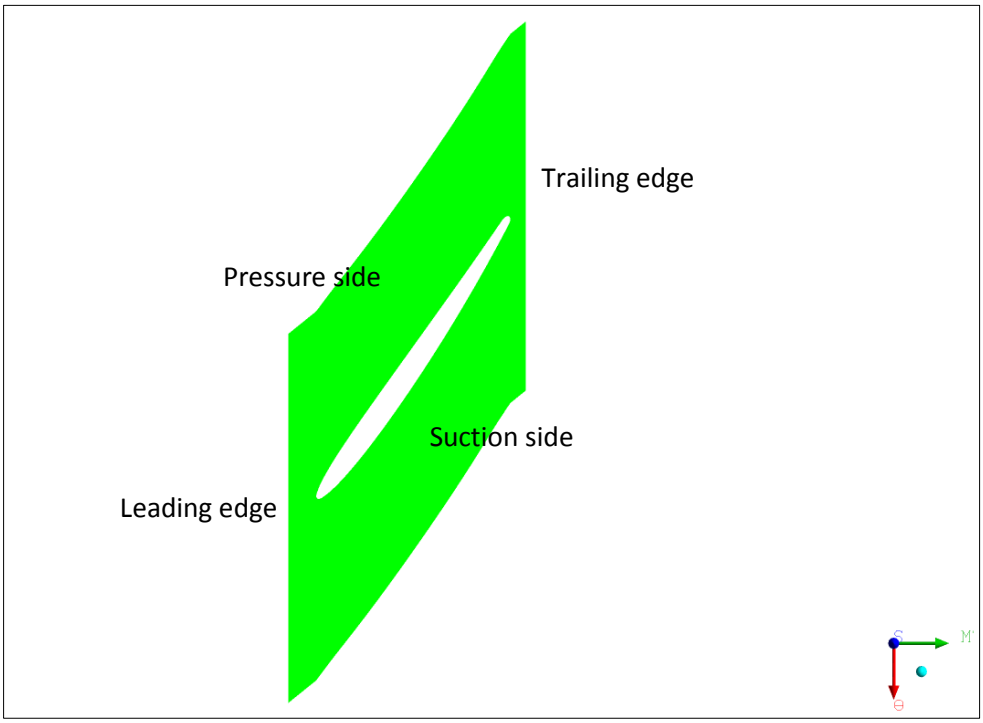


**Figure 7.7 A sliced surface of the blade at mid span in 2D plane.**

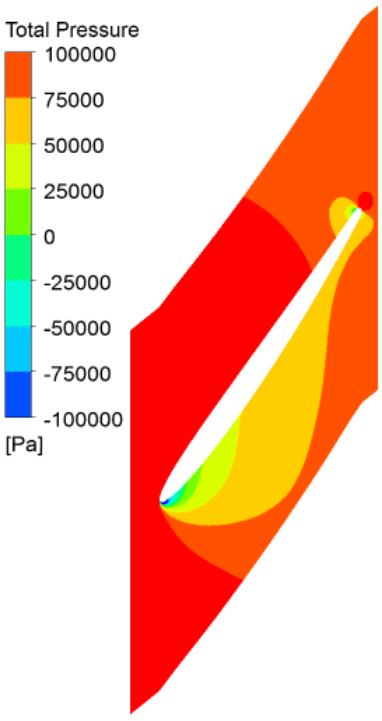


a. 1827 RPM

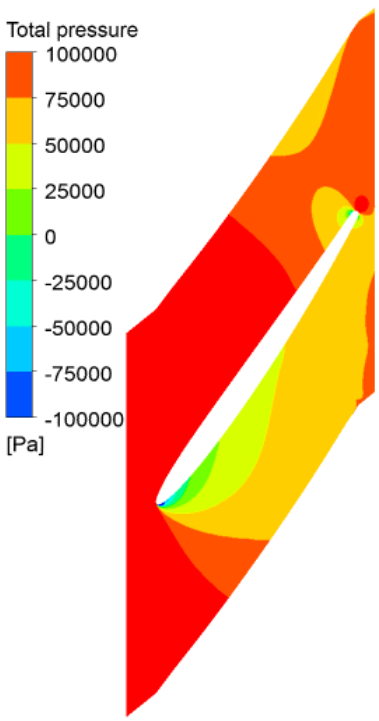


b. 2259 RPM

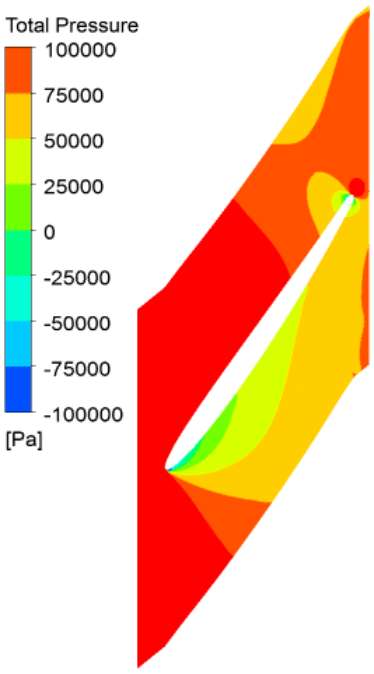


c. 2730 RPM

**Figure 7.8 Pressure contours at the mid span of the runner blade at three operating regimes**

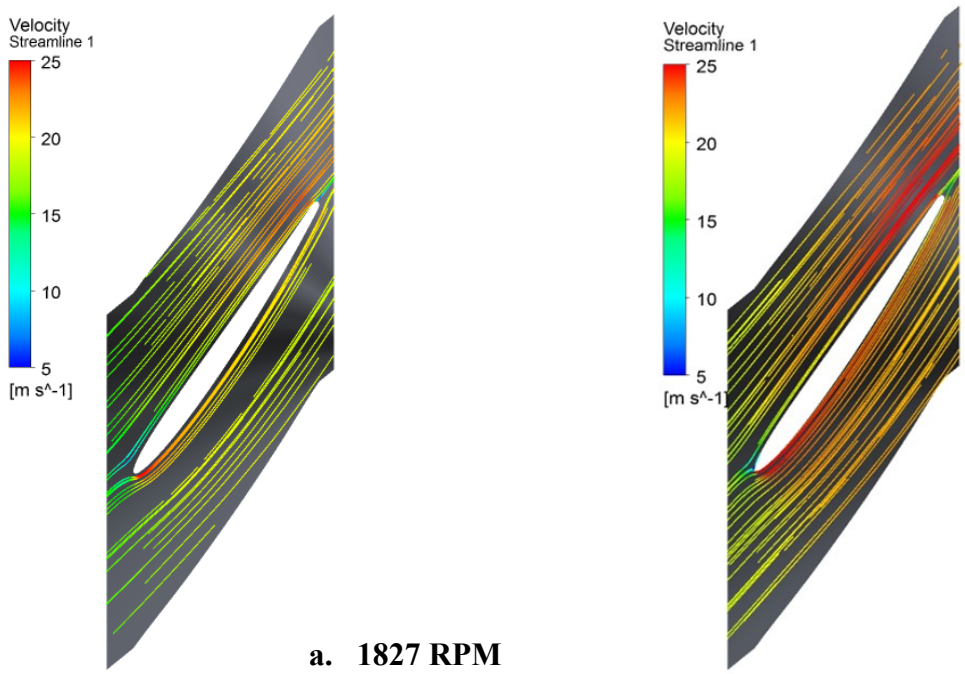


**a. 1827 RPM**

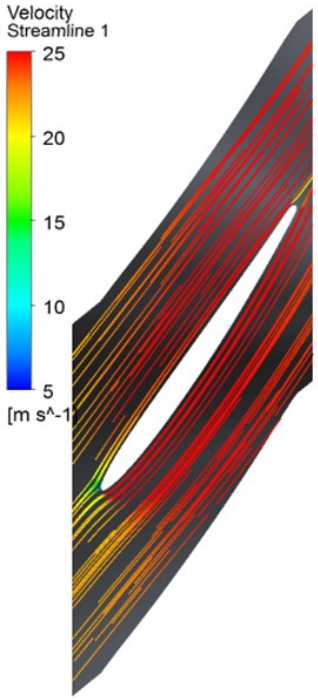


**Figure 7.9 Velocity streamlines at the mid span of the runner blade at three operating regimes**

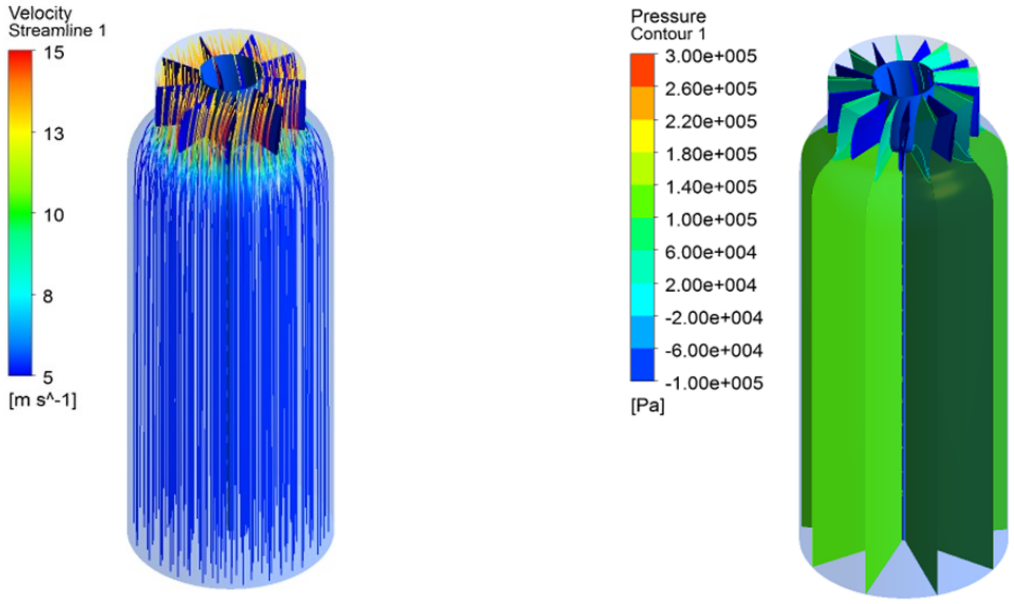


**Figure 7.10 Velocity streamline and pressure contour at the inlet and stator blade for RPM 2259**

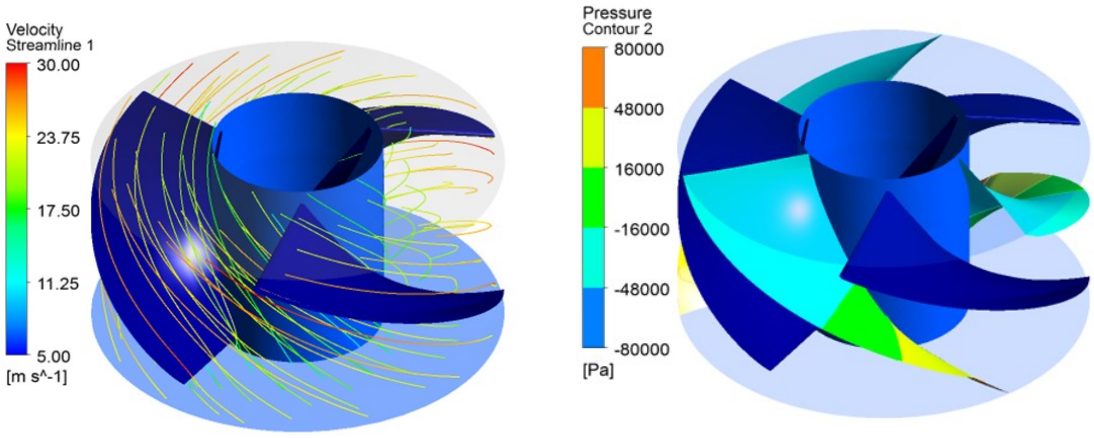


**Figure 7.11 Velocity streamlines and pressure contours in the rotor for RPM 2259**

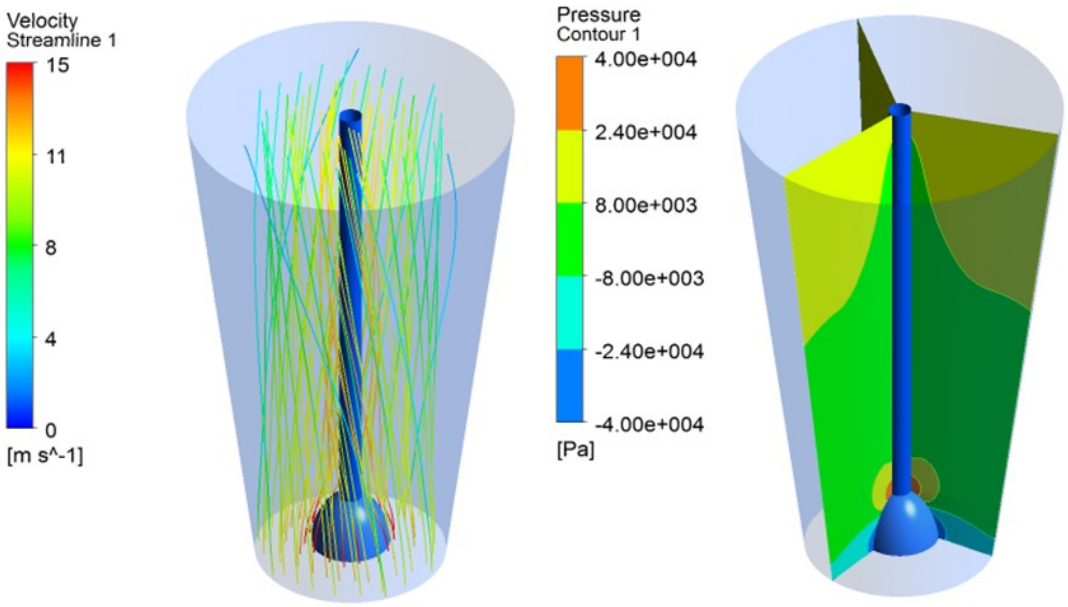


**Figure 7.12 Streamlines and pressure contours on draft tube for RPM 2259**

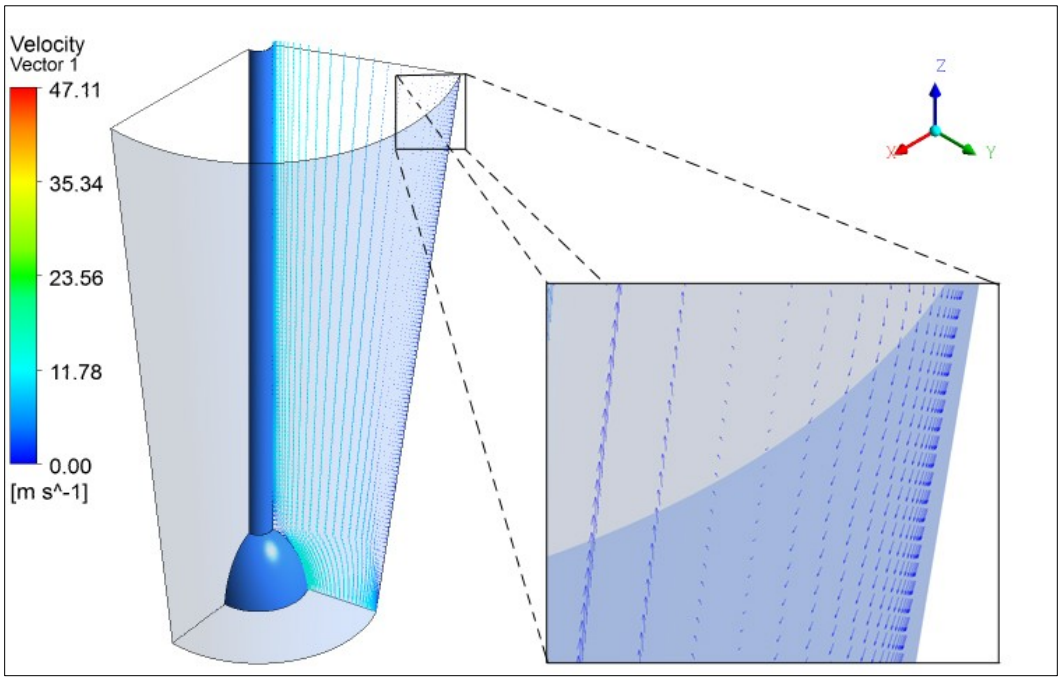


**Figure 7.13 Velocity vectors in draft tube showing backflow for RPM 2259**

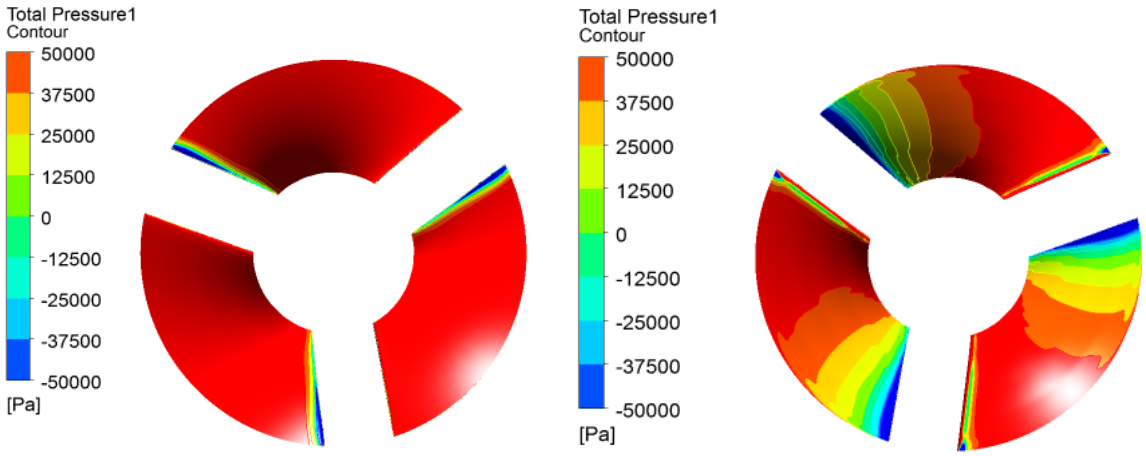


**Figure 7.14 Pressure contours at pressure side and suction side of a runner for RPM 2259.**

It can be seen that velocity increases with the increase in RPM which is due to increases in discharge. It is seen that the flow is smooth for all three cases. As we know that the best efficiency point for 30 feet of head is at RPM 2259 where the runner is generating maximum power, the detailed plots are shown for the case.

3D plots for streamline and pressure contours for RPM 2259 have been shown in Figures 7.10-7.14. Figure 7.10 and 7.11 shows that velocity increases and pressure decreases as flow moves from the stator blade to runner blade. It depicts that velocity is higher at the suction side of the blade so the pressure is decreased and velocity is less at the pressure side so velocity is greater at that side. Figure 7.12 shows the streamline and pressure contour inside the draft tube. The streamline shows vorticity development in the draft tube. Figure 7.14 shows the pressure contour at pressure side and suction side of the runner blade. It is seen clearly that the negative pressure zone is observed on the suction side of the blade.

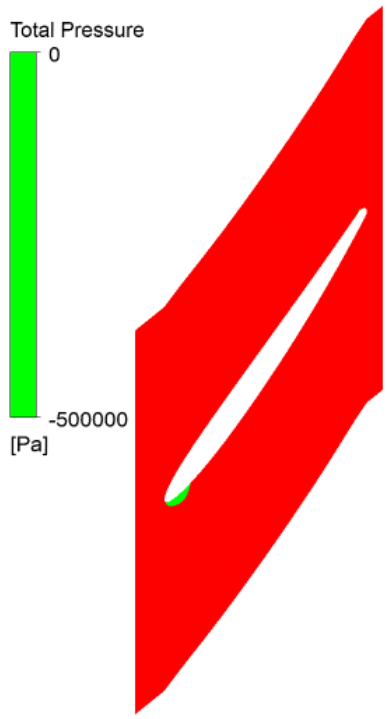


a. 1821837 RPM

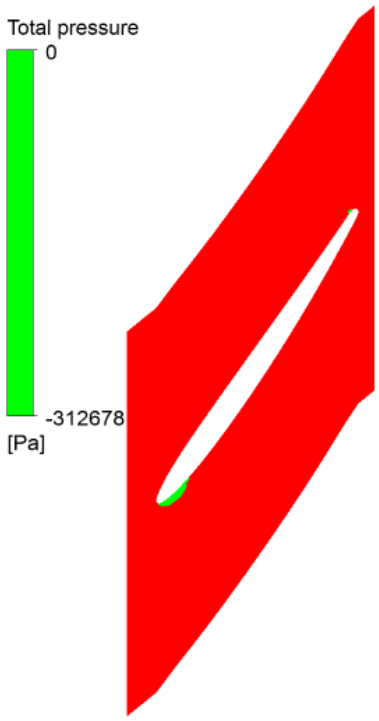


b. 2259 RPM

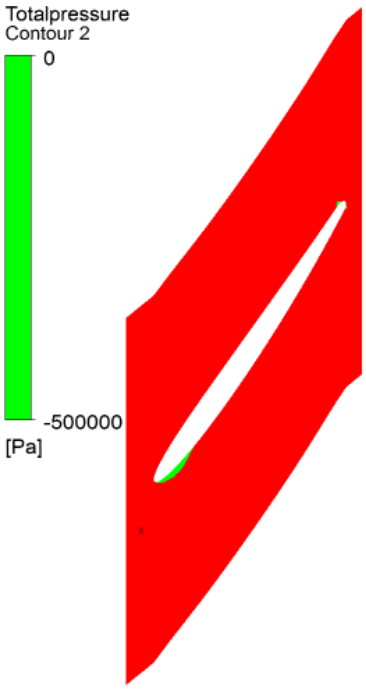


c. 2730 RPM

**Figure 7.15 Contours showing cavitation for three operating regimes**

Figure 7.15 shows the pressure contours on the mid span of the runner blade and indicates negative pressure formation at the suction side of the leading edge of the blade. Negative pressure distribution on the suction side of the blade is mainly due to the dynamic action of the blade. High velocity of the water on this location creates a low-pressure area. When local static pressure becomes less than the vapor pressure, cavitation will take place. It is evident from the contours plot that there is an occurrence of cavitation. As RPM increases with increasing discharge, negative pressure is developing on the leading edge as well as on the trailing edge of the blade.

## 7.1 Limitations

Several assumptions have been made while carrying out the CFD analysis. Thus this study of comparing the experimental values with CFD is not without limitations. Following are the constraints that were raised while carrying out this project.

3) The geometry of the turbine for simulation was a simplified geometry with no fillet at the blades. Also, the geometry of an inlet pipe was an inch shorter than what was tested in the laboratory.
4) A portion of the inlet and draft tube was made a solid shaft to reduce skewness of the mesh at curved locations.
5) Though $Y^+$ values need to be less than 200 according to shear stress transport model, at a few locations these values were obtained to be around 1500.
6) Steady state analysis carried out during current the CFD simulation gives the solution with averaging of the fluxes as they move from rotating to non-rotating

domain. Though it is pretty standard to perform steady state analysis to compare with the experimental results, it is evident that transient analysis is the best approach to obtain precise solution. However, though transient simulation can give accurate results as compared to steady state, they are much more expensive in terms of the required computational time and resources.

7) Cavitation could be one of the reasons for power to decrease at overload condition which was not accounted for in the simulation.

### 7.2 Summary

The performance of the turbine can be best evaluated by the numerical simulation as experimental evaluation consumes time and money. Another advantage of numerical simulation is that the experimental results can be verified if there is a geometrical similarity between experimental and numerical geometry. Numerical simulation of a horizontal Kaplan turbine was presented in this report with total pressure inlet and static pressure outlet as boundary conditions and solved using commercial software ANSYS CFX with shear stress transport model. Required mesh resolution was achieved by grid generation in ANSYS Turbogrid and Pointwise Gridgen. Boundary conditions for the simulations were imposed with the data gathered from the experiment conducted in the Hydraulic annex. Five simulations were run with the data from the experiment for 30 feet of head across the runner. With the plot of RPM vs. power, it was observed that the power developed at the optimum point was matching with the power generated from the experiment whereas for the overload condition it was over predicting. Further simulations were conducted for the cases when the turbine was

making maximum power for head varying from 20 feet to 50 feet. From the graph plotted between RPM and variables power, torque and discharge, it was observed that the simulation value follows the trend for RPM vs. Power and RPM vs. discharge and for RPM vs. torque the values compared well for four cases only. The variation in values might be due to discretization error of the domain and geometrical dissimilarity of the inlet pipe. For the case of 30 feet of head where simulation was making over prediction with the experimental value might be due to losses that have not been accounted for properly in the simulation. The pressure contour on the mid span of the runner blade shows presence of negative pressure developed at the suction side of the leading edge of the blade. This depicts cavitation formation during the operation of the turbine. Hence, to account for losses caused by cavitation, two phase flow should be conducted. Also, the steady state assumption might have averaged the losses in the turbine runner which could be the reason for the over predicted power for the overload condition. Future works are discussed in the following chapter that can be conducted for better prediction of the turbine efficiency.

# CHAPTER 8 FUTURE WORK

This research was carried out with limitations which could be reduced if similar nature of work is conducted in future. From the findings of this research, it is assumed that more accurate results could have been achieved if we had sufficient time to run unsteady analysis as well. Following can be some works that can be done in future in order to get results with minimum errors.

1) Although we know that the flow in the turbine is unsteady in nature, steady state has been assumed due to time constraints. Transient simulation with total nodes of 1.3 million may take about 10 days to reach a converged solution. Therefore, further studies can be done with transient simulation for the turbine.
2) Geometrical similarity is required for setting up the same boundary conditions. The inlet pipe of the numerical geometry was 1 inch smaller than what was tested in the lab. This might have caused inaccuracy in the result. Therefore, there should be similitude between lab and CFD geometry.
3) Negative pressure was developed on the suction side of the blade which is lower than the vapor pressure of the fluid at 20° C. With critical cavitation calculation it was observed that there is an occurrence of cavitation in the runner blade. Hence, it may be desirable to simulate the flow with a cavitation model to account for the losses caused by it.

## REFERENCES

ANSYS CFX 12 Documentation, ANSYS Inc.,2010

"Best Practice Guidelines for Turbo Machinery." http://www.scribd.com/doc/53461341/Best-Practice-Guidelines-for-Turbo-Machinery.

Brost, V., A. Ruprecht, and M. Maihöfer. 2003. "Rotor-stator Interactions in an Axial Tur-bine, A Comparison of Transient and Steady State Frozen Rotor Simulations." In *Conference on Case Studies in Hydraulic Systems-CSHS03, Belgrade*.

"Bureau of Reclamation Homepage." http://www.usbr.gov/.

Čarija, Z., Z. Mrša, and S. Fućak. 2008. "Validation of Francis Water Turbine CFD Simulations." *Strojarstvo* 50 (1): 5–14.

Drtina, P., and M. Sallaberger. 1999. "Hydraulic Turbines—basic Principles and State-of-the-art Computational Fluid Dynamics Applications." *Proceedings of the Institution of Mechanical Engineers, Part C: Journal of Mechanical Engineering Science* 213 (1): 85–102.

F R Menter,1994 "Two equation eddy- viscosity turbulence models for engineering applications."

Gagnon, J. M., and C. Deschênes. 2007. "Numerical Simulation of a Rotor-Stator Unsteady Interaction in a Propeller Turbine." *CFD Society of Canada. Toronto, Canada*.

Gagnon, J. M., C. Deschênes, G. D. Ciocan, and M. Iliescu. 2008. "Numerical Simulation and Experimental Investigation of the Flow in an Axial Turbine." In *24th AIRH Symposium on Hydraulic Machinery and System, Foz Do Iguassu, Brazil, Paper*.

Grigori Krivchenko. 1994. *Hydraulic Machines : Turbines and Pumps*. second ed. http://trove.nla.gov.au/work/10021182.

Hart, D., D. Whale, and others. 2007. "A Review of Cavitation-erosion Resistant Weld Surfacing Alloys for Hydroturbines." *Eutectic Castolin Web News Publications*.

Ivanshchenko,A.,Bennett E., 2012 "Horizontal Kaplan turbine design and CFD analysis"

Jain, S., R. P. Saini, and A. Kumar. 2010. "Cfd Approach for Prediction of Efficiency of Francis Turbine."

John D Anderson. 1995. *Computational Fluid Dynamics: The Basics with Application*.

Kokubu, K., S. W Son, T. Kanemoto, and Y. D Choi. 2011. “Internal Flow Analysis on a Micro Cross-Flow Type Hydro Turbine at Very Low Specific Speed Range.”

Laín, S., M. García, B. Quintero, and S. Orrego. 2010. “CFD Numerical Simulations of Francis Turbines.” *Revista Facultad De Ingeniería Universidad De Antioquia* (51): 24–33.

Liu, ShuHong, Jie Shao, ShangFeng Wu, and YuLin Wu. 2008. “Numerical Simulation of Pressure Fluctuation in Kaplan Turbine.” *Science in China Series E: Technological Sciences* 51 (8) (July 6): 1137–1148. doi:10.1007/s11431-008-0159-9.

Longo J, Lyons T and Weber L, 2011. "Laboratory tests of the ATS integrated hydroelectric turbine/generator prototype

“Model_advice.pdf.” http://hikwww2.fzk.de/hik/orga/hlr/AIX/software/cfx/flow/cfx_models/model_advice.pdf.

Motycak, L., A. Skotak, and J. Obrovsky. 2010. “Conditions of Kaplan Turbine Cfd Analysis.”

Nilsson, H., and L. Davidson. 2003. “Validations of CFD Against Detailed Velocity and Pressure Measurements in Water Turbine Runner Flow.” *International Journal for Numerical Methods in Fluids* 41 (8): 863–879.

Prasad Vishnu, V.K Gahlot, and P Krishnamachar. 2009. “CFD Approach for Design Optimization and Validation for Axial.” *Docstoc.com*.

“Y+ Calculator.” http://www.pointwise.com/yplus/.